TWO-DIMENSIONAL BRIGHT SOLITONS IN DIPOLAR BEC WITH TILTED DIPOLES

A thesis submitted towards partial fulfilment of
BS-MS Dual Degree Programme

by

MEGHANA RAGHUNANDAN

under the guidance of

Dr. REJISH NATH

Assistant Professor

Indian Institute of Science Education and Research Pune

Certificate

This is to certify that this thesis entitled **Two-Dimensional Bright Solitons in Dipolar BEC with tilted dipoles** submitted towards the partial fulfilment of the BS-MS dual degree programme at the Indian Institute of Science Education and Research Pune represents original research carried out by **Meghana Raghunandan** at the **Indian Institute of Science Education and Research, Pune**, under the supervision of **Dr. Rejish Nath** during the academic year 2014-2015.

Student
Meghana
Raghunandan

Supervisor
Dr. Rejish Nath

Declaration

I hereby declare that the matter embodied in the report entitled **Two-Dimensional Bright Solitons in Dipolar BEC with tilted dipoles**, are the results of the investigations carried out by me at the Department of Physics, Indian Institute of Science Education and Research Pune, under the supervision of Dr. Rejish Nath and the same has not been submitted elsewhere for any other degree.

Student
Meghana
Raghunandan

Supervisor
Dr. Rejish Nath

Acknowledgements

I would like to offer my sincere thanks to Dr. Rejish Nath, without whose guidance, this thesis would not have been possible. I am grateful for those times when you offered valuable advice concerning not only the research project but also other aspects of life. When I started this project I had little idea of how research in Physics is actually done. But working with you has helped me learn the ways of research. The constant motivation and guidance you have given me throughout this project has really made me meticulous in my work.

I am very thankful to Dr. Paolo Pedri for agreeing to be on my TAC, Dr. Kazimierz Łakomy, whose notes gave me a head start on the project, and also to Prof. Dr. Luis Santos, a great collaborator.

I would like to take this opportunity to extend my gratitude towards each of the faculty members here at IISER Pune who have always been so warm and friendly.

I also thank Ms. Chinmayee Mishra, who is currently pursuing her doctoral studies at IISER. The many discussions we had really helped me in having a better understanding of the subject. Also, many thanks for making the couple of plots for me!

I would like to thank my friends here at the institute and elsewhere who have always been with me through thick and thin times.

Lastly, I thank my parents from the bottom of my heart, my father especially, for helping me develop a passion for Physics from the very beginning and my mother who has always been my strong support. I would also like to thank my little brother and the rest of my family.

This work was supported by INSPIRE grant from the Department of Science and Technology (DST), Government of India.

To Amma, Appa, Mithun, and Thatha.

Contents

List of Figures

Chapter 1

Introduction

In the last two decades, the physics of *ultracold atoms* has attracted a number of physicists whose work has resulted in a tremendous progress both in the theoretical and experimental fields. Ultracold atoms find direct applications in many aspects of physics namely, condensed matter physics, non-linear physics, quantum optics, and quantum information. Various cooling and trapping methods were developed since the '70s, and in 1980, laser based techniques such as laser cooling and magneto-optical trapping were found. These discoveries have been awarded with several Nobel Prizes in Physics.

In the year 1925, Albert Einstein, based on a paper by Satyendra Nath Bose, predicted the occurrence of phase transition in a gas of non-interacting atoms which leads to the condensation of atoms in the lowest energy, a consequence of quantum statistical effects. After the discovery of superfluidity in liquid Helium, F. London proposed that superfluidity could be a manifestation of Bose-Einstein condensation (BEC). The first microscopic theory of interacting Bose gases was given by Bogoliubov in 1947 and later in the years 1951-1956, Landau and Lifshitz, and, Penrose and Onsager [36] introduced the concept of non-diagonal long-range order. Despite the huge literature on the theory of BEC, the initial experiments opened up a series of new questions. Though early experimental studies on dilute atomic gases began in 1970s, focusing on spin-polarized hydrogen atoms, the first experimental realizations of BEC were seen only in 1995 in the atoms of ^{87}Rb [5], ^{23}Na [14] and ^{7}Li [8]. BECs were then observed in other atomic species such as spin-polarized hydrogen, metastable ^{4}He [15] and in ^{41}K [30] only in 2001.

The most important feature of trapped Bose gases is their inhomogeneity, which allows the investigation of many physical quantities that was not possible in previous experiments on liquid Helium. In particular, BECs show up not only in the momentum space but also in coordinate space which allows making direct experimental investigation of the condensate feasible [37].

1.1 Bose-Einstein condensation

The occurrence of Bose-Einstein condensation, a new state of matter for bosons, was first predicted by Albert Einstein [17] motivated by the letter on photon-statistics written by Satyendra Nath Bose [7]. BEC is a phenomenon in which a finite fraction of the total number of bosons occupy the lowest energy quantum state, provided the system is below the critical temperature $T_c = \frac{2\pi\hbar^2}{mk_B}\left(\frac{n}{\zeta(3/2)}\right)^{2/3}$ [20]. This macroscopic occupation of the single-particle state is observed when the phase-space density is such that $n\lambda^3 > \zeta(3/2)$. Here, $\lambda = \sqrt{\frac{2\pi\hbar^2}{mk_BT}}$ is the thermal de-Broglie wavelength with m being the mass of the atom, k_B the Boltzmann constant, T the temperature and $\zeta(3/2) = 2.312$ is the Riemann- zeta function at $3/2$.

The concepts of non-diagonal long range order and spontaneous breaking of gauge-symmetry are the basic concepts underlying the phenomenon of BEC [37]. Consider the one-body density matrix of a uniform and isotropic system of N particles occupying a volume V in the absence of external potentials, $n^{(1)}(\mathbf{r},\mathbf{r}',t) = \langle\hat{\Psi}^\dagger(\mathbf{r},t)\hat{\Psi}(\mathbf{r}',t)\rangle$ where, $\Psi^\dagger(\mathbf{r},t)$ and $\Psi(\mathbf{r},t)$ are field operators creating and annihilating a particle at $\mathbf{r}$ respectively. In thermodynamic limit $(N, V \to \infty)$, the one-body density matrix depends only on the relative distance $\mathbf{s} = \mathbf{r} - \mathbf{r}'$:

$$n^{(1)}(s) = \frac{1}{V}\int d\mathbf{p}\; n(\mathbf{p})\; e^{-i\mathbf{p}\cdot\mathbf{s}/\hbar} \tag{1.1}$$

where $\mathbf{p}$ is the momentum. For normal momentum distribution, the one-body density matrix vanishes as $s \to \infty$ but if instead the momentum distribution exhibits a singular behaviour, $n(\mathbf{p}) = N_0\delta(\mathbf{p}) + \tilde{n}(\mathbf{p})$, the density matrix does not vanish at large distances but tends to a finite value $n_0 = N_0/V$ thus exhibiting long-range order.

Inter atomic interactions play a very important role in the physics of atomic condensates. The short-range interactions depend predominantly on the s-wave scattering length a [13]. Repulsive short-range interaction, characterized by positive scattering length, results in a stable BEC irrespective of trap, dimension, or number of atoms. Attractive short-range interaction $(a < 0)$ results in a collapse of the atoms of the condensate in two-dimension (2D) and three-dimension (3D), however the presence of trap can stabilize the condensate if the number of atoms is below a critical value N_{cr} which depends on the geometry of the trap, and can be calculated using the Gross-Pitaevskii equation. Fig. 1.1 shows the energy per particle (in units of $\hbar\omega$), as a function of the variational parameter w of the Gaussian ansatz $\psi(\mathbf{r}) = (N/\pi^{3/2}a_{ho}^3 w^3)^{1/2}\exp\left(-r^2/2a_{ho}^2w^2\right)$ for the ground state of a BEC in spherical trap. We see that the local minimum disappears at $N = N_{cr}$. For a spherical trap, this happens at $\frac{N_{cr}|a|}{a_{ho}} = 0.575$. [37].

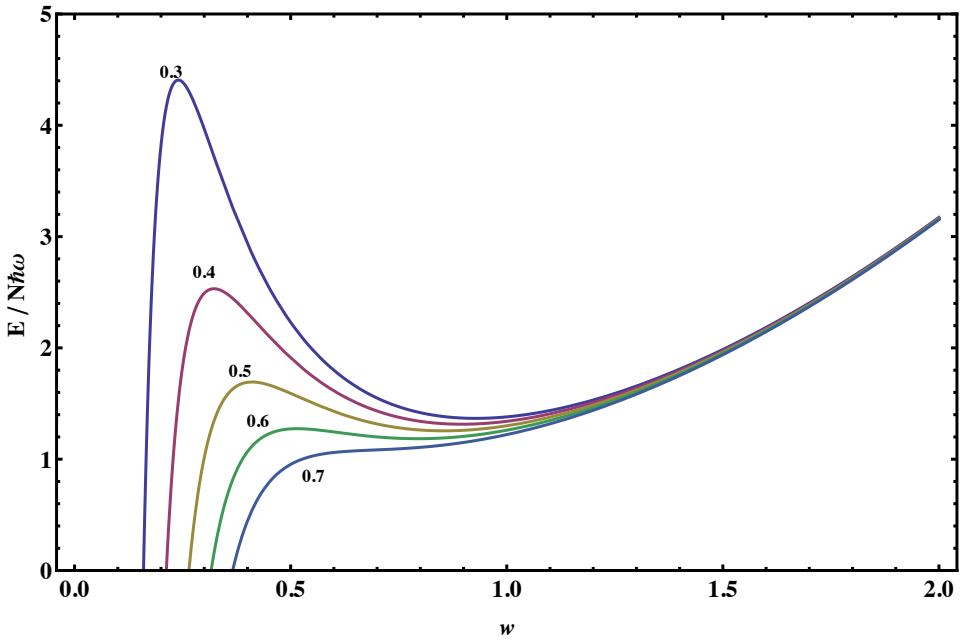

Figure 1.1: Energy per particle (in units of $\hbar\omega$) as a function of the variational parameter w for a BEC with attractive short-range interactions in a spherical trap, plotted for various values of $N|a|/a_{ho}$. The local minimum disappears at $N = N_{cr}$

The presence of dipole-dipole interactions changes the whole picture as we shall discuss in chapter 2.

1.1.1 Gross-Pitaevskii Equation

Consider a nonuniform system of N bosons with mass m interacting via a two-body potential $V(\mathbf{r}-\mathbf{r}')$, in an external trap V_{ext}. In the language of second quantization, the system is described by the Hamiltonian [13]

$$\begin{aligned}\hat{H} &= \int d\mathbf{r}\hat{\psi}^\dagger(\mathbf{r})\left[-\frac{\hbar^2}{2m}\nabla^2 + V_{ext}(\mathbf{r})\right]\hat{\Psi}(\mathbf{r}) \\ &\quad + \frac{1}{2}\int d\mathbf{r}d\mathbf{r}'\hat{\Psi}^\dagger(\mathbf{r})\hat{\Psi}^\dagger(\mathbf{r}')V(\mathbf{r}-\mathbf{r}')\hat{\Psi}(\mathbf{r}')\hat{\Psi}(\mathbf{r}) \qquad (1.2)\end{aligned}$$

Employing the mean-field description formulated by Bogoliubov (1947), we separate the condensate contribution from the bosonic field operator.

$$\hat{\Psi}(\mathbf{r},t) = \Psi(\mathbf{r},t) + \hat{\Psi}'(\mathbf{r},t) \qquad (1.3)$$

where $\Psi(\mathbf{r},t) \equiv \langle\hat{\Psi}(\mathbf{r},t)\rangle$ is the condensate wave function and $\hat{\Psi}'(\mathbf{r},t)$ is a small perturbation. We write the time-evolution of the field operator $\hat{\Psi}(\mathbf{r},t)$

using the Heisenberg equation.

$$\begin{aligned} i\hbar\frac{\partial\hat{\Psi}(\mathbf{r},t)}{\partial t} &= [\hat{\Psi}(\mathbf{r},t),\hat{H}] \\ &= \left[-\frac{\hbar^2}{2m}\nabla^2 + V_{ext} + \int d\mathbf{r}'\hat{\Psi}(\mathbf{r},t)V(\mathbf{r}-\mathbf{r}')\hat{\Psi}(\mathbf{r}',t)\right]\hat{\Psi}(\mathbf{r},t) \end{aligned} \tag{1.4}$$

Since we consider only short-range contact potential characterized by the s-wave scattering length a, we substitute $V(\mathbf{r}-\mathbf{r}') = g\delta(\mathbf{r}-\mathbf{r}')$ [13] where $g = 4\pi\hbar^2 aN/m$. Replacing the field operator $\hat{\Psi}$ with classical field Ψ in Eq. 1.4, we obtain the following closed equation for the order parameter.

$$i\hbar\frac{\partial\Psi(\mathbf{r},t)}{\partial t} = \left[-\frac{\hbar^2}{2m}\nabla^2 + V_{ext}(\mathbf{r}) + g|\Psi(\mathbf{r},t)|^2\right]\Psi(\mathbf{r},t) \tag{1.5}$$

Eq. 1.5 is called the time-dependent Gross-Pitaevskii equation (GPE) and was derived independently by Gross (1961 and 1963) and Pitaevskii (1961). It is also known as the Non-Linear Schrödinger Equation (NLSE) and is the main theoretical tool used in the study of non-uniform Bose gases at low temperature. The GPE is also widely used in various fields of physics namely, non-linear optics, plasma physics etc.

1.1.2 Elementary Excitations

The first excitation spectrum of a weakly interacting gas of bosons was calculated by Bogoliubov. It plays an important role in our understanding of superfluidity of Bose gases. Since the first experimental observation of BEC, there has been an increased study of elementary excitations in these systems and several theoretical works have been made exploring the behaviour of trapped Bose gases.

We begin by calculating the dispersion relation $\epsilon(\mathbf{k}) = \hbar\omega(\mathbf{k})$ of the Bogoliubov excitations of the BEC by linearizing the time dependent GPE 1.5 around the ground state $\psi(\mathbf{r})$. We consider solutions of the form

$$\Psi(\mathbf{r},t) = e^{-i\mu t/\hbar}\left[\psi(\mathbf{r}) + u(\mathbf{r})e^{-i\omega t} + v^*(\mathbf{r})e^{i\omega t}\right] \tag{1.6}$$

where u and v are the amplitudes of small perturbations with Bogoliubov frequency ω. We keep only the linear terms in u and v in the GPE 1.5 to obtain the following equations.

$$\hbar\omega u(\mathbf{r}) = [H_0 - \mu + 2g\psi^2(\mathbf{r})]u(\mathbf{r}) + g\psi^2\mathbf{r}v(\mathbf{r}) \tag{1.7}$$

$$-\hbar\omega v(\mathbf{r}) = [H_0 - \mu + 2g\psi^2(\mathbf{r})]v(\mathbf{r}) + g\psi^2\mathbf{r}u(\mathbf{r}) \tag{1.8}$$

with $H_0 = -(\hbar^2/2m)\nabla^2 + V_{ext}(\mathbf{r})$. These coupled equations 1.7 and 1.8 let us calculate the eigenfrequencies ω and their energies $\hbar\omega$. This was introduced by Pitaevskii in 1961. One can also take the quantum- mechanical approach

to derive the same. Purely real values for ω implies stability of the ground state ψ whereas non-zero imaginary part of ω suggests instability of Ψ.

The amplitudes u and v for a *uniform gas* are plane waves of the form $u(\mathbf{r}) = u_0 e^{i\mathbf{k}\cdot\mathbf{r}}$ and $v(\mathbf{r}) = v_0 e^{i\mathbf{k}\cdot\mathbf{r}}$ and the dispersion law takes the famous Bogoliubov form

$$(\hbar\omega)^2 = \left(\frac{\hbar^2 k^2}{2m}\right)\left(\frac{\hbar^2 k^2}{2m} + 2gn\right) \tag{1.9}$$

where $\mathbf{k}$ is the excitation wavefactor and $n = |\psi|^2$ is the density. At large momenta this reduces to the free- particle energy $\hbar^2 k^2/2m$ and at small momenta, Eq. 1.9 results in phonon dispersion $\omega = ck$ with $c = \sqrt{gn/m}$ being the sound velocity.

Landau's criteria for Superfluidity:

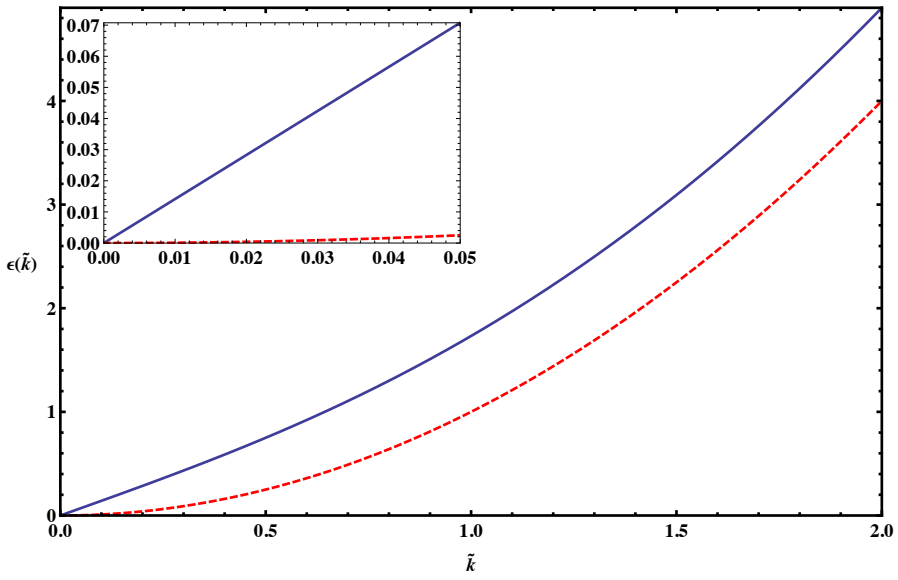

Figure 1.2: Plot of Bogoliubov excitations $\epsilon(\tilde{k})$ as a function of $\tilde{k}$ for a weakly interacting Bose gas (blue solid) and ideal Bose gas (red dashed). (Inset: Magnified plot showing the lower $\tilde{k}$ region). $\dfrac{d\epsilon(k)}{dk} \to 0$ at lower $\tilde{k}$ values for ideal Bose gas, making the critical velocity $v_r = 0$, thus exhibiting no superfluidity.

When the velocity of a fluid v is such that

$$v < v_{cr} \tag{1.10}$$

where, $v_{cr} = \min_{\mathbf{k}} \dfrac{\epsilon(\mathbf{k})}{|\mathbf{k}|}$, there will be a persistent flow without friction resulting in superfluidity. Thus, Eq. 1.10 gives the Landau's criteria for superfluidity. Fig. 1.2 shows $\epsilon(\tilde{k})$ ($\mathbf{k}$ scaled by $\tilde{k} = k\xi$ where ξ is the healing

length) as a function of $\tilde{k}$ for a weakly interacting Bose gas and ideal Bose gas. For an ideal Bose gas, at low $\tilde{k}$ values, $\frac{d\epsilon(\tilde{k})}{d\tilde{k}} \to 0$, making the critical velocity $v_{cr} = 0$. This implies that though ideal Bose gases can form BECs, they can never exhibit superfluidity. However, weakly interacting Bose gases satisfy the Landau criteria for superfluidity at zero temperature, with the critical velocity being the velocity of sound [37]. Thus, not all BECs can be superfluids.

1.2 Solitons in BEC

Soliton, or a solitary wave, which is an exact analytical solution of the time-dependent GPE, is a localized disturbance which propagates without changing its form. The origin of formation of such solitons lies in the non- linearity and the non- locality present in the media. They preserve their form as the non-linearity and dispersion effects cancel each other out. Solitons were first observed and described by a Scottish engineer named John Scott Russell in 1845 while conducting experiments to determine the most efficient design for canal boats [32]. It was only in mid 1960s that Russell's early idea was appreciated, when scientists began to study nonlinear wave propagation. Today, solitons appear in almost every field: hydrodynamics, meteorology, nonlinear optics, laser physics, plasma physics, particle physics and many more. Solitons in BEC are typically of two types, *dark solitons* that are formed in condensates with repulsive interactions, and, *bright solitons* [37], formed in the case of attractive interactions. In this thesis we shall focus only on bright solitons.

1.2.1 1D Bright Solitons

In BECs with only short-range contact interaction, stable solitons are found only in one-dimension [1]. This can be seen by observing the energy E of a self-attractive BEC ($g_D < 0$) in dimension D confined by a harmonic trap.

$$E = \int \left[\frac{\hbar^2}{2m} |\psi|^2 + V|\psi|^2 + \frac{g_D}{2}|\psi|^4 \right] d^D\mathbf{r}$$

If we consider a BEC with size L and attractive contact interaction, we see that the kinetic term in the energy expression behaves as $1/L^2$, the trap as L^2, and the contact interaction term behaves as $1/L^D$. Thus,

$$E \sim \frac{C_{kin}}{L^2} + C_{pot}L^2 + \frac{C_{int}}{L^D}.$$

In the absence of the external trap, for $D = 2$ both kinetic and interaction energy scale as L^{-2} and the system either expands (when kinetic energy dominates the interaction energy) or collapses (when interaction dominates over kinetic energy). Similarly, for $D = 3$, the absence of local minimum in

the energy E (Fig. 1.3) indicates that the system either expands or collapses for any values of g.

When $D = 1$, the dispersion and attractive inter-atomic interaction balance each other resulting in the formation of a stable soliton. As seen in Fig. 1.3(a), the energy functional has a minimum. The quasi-1D GPE

$$i\hbar\frac{\partial\psi(z,t)}{\partial t} = \left[-\frac{\hbar^2}{2m} + g_{1D}|\psi(z,t)|^2\right]\psi(z,t) \tag{1.11}$$

possesses a bright solitonic solution of the form [26]

$$\psi(z,t) = \psi_0\,\mathrm{sech}[(z-vt)/\zeta]\,\exp[i(kz-\omega t)] \tag{1.12}$$

where, $n_0 = |\psi_0|^2$ is the central density, v is the velocity of the soliton, $\zeta = \hbar/\sqrt{m|g|n_0}$ is the spatial width of the soliton, k is the soliton wave number and ω is the frequency.

The very first bright solitons were observed in experiments performed at Rice University [43] and at the Ecole Normale Supérieure in Paris [21]. Both these groups have reported to observe 1D bright solitons in ^{7} Li condensates. Fig. 1.4 shows the soliton train formation.

1.2.2 Multi-dimensional Solitons

The last decades have witnessed intensive investigations, both theoretical and experimental, on multi-dimensional bright solitons in various non-linear setups, especially in systems possessing nonlocal-nonlinearity (NL-NL) [42, 6, 4] such as atomic Bose-Einstein condensates (BECs) with permanent [35, 44] or induced dipole moments [28], photo refractive materials [22], nematic liquid crystals [11, 33] and others [24, 9, 27]. 2D optical bright solitons [12] as well as 3D light bullets [29] in a non-local medium have been reported. In addition, the non-locality also induces long-range interactions between solitons and hence significantly influence the inter-soliton collisional dynamics [35, 22, 31, 16] and may lead to the formation of soliton complexes [23, 41]. The existence of bright solitons in condensates has been demonstrated experimentally in quasi-1D alkali-atom BECs, however the 2D counterpart still remains an open challenge. But the achievements of the dipolar condensates [19, 2, 25] show promising possibilities of realizations of 2D bright solitons.

1.3 Dipolar BEC

The experimental productions of BECs of Chromium [19], Erbium [2], and Dysprosium [25] atoms (they have large magnetic moment of $m = 6\mu_B, 7\mu_B$, and, $10\mu_B$ respectively, where μ_B is the Bohr magneton) have given rise to growing interests in dipolar condensates. It is interesting that application of feshbach resonances may help suppressing short-range interactions resulting

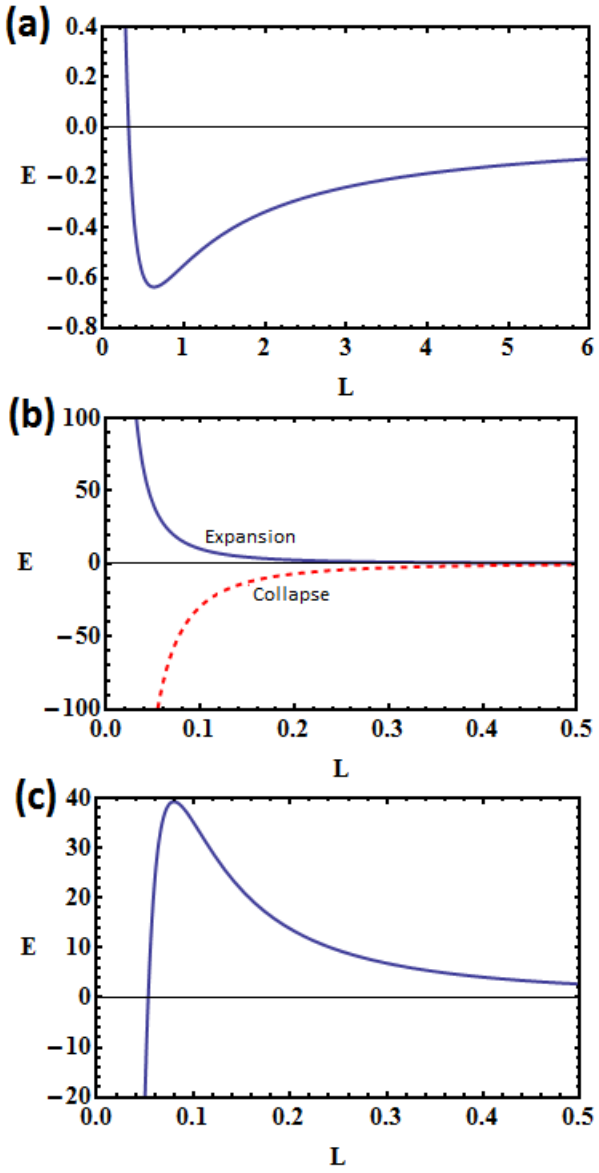

Figure 1.3: Energy as a function of the variational parameter L (Gaussian width of attractive BEC in the absence of a trap) for (a) $D = 1$, with $g_1 = 0.1$, (b) $D = 2$, with $g_2 = 1$ (upper curve) and $g_2 = 2$ (lower curve) and, (c) $D = 3$ in the absence of a trap. The energy shows a minimum only in the $D = 1$ case resulting in stable solitons, whereas $D = 2, 3$ results in instability of the condensate.

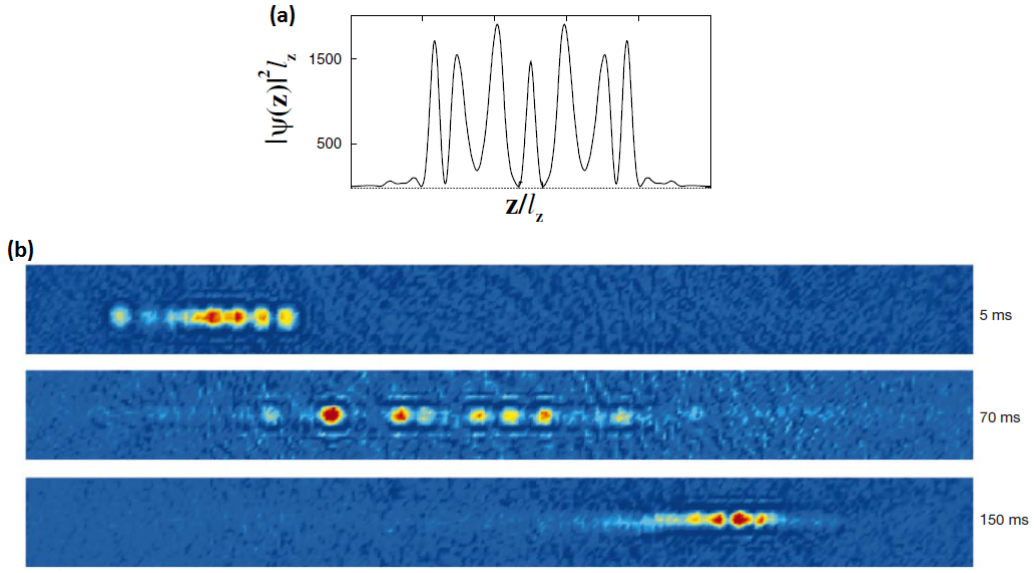

Figure 1.4: Soliton train formation. (a) The solid curve is the density and the dashed curve is the phase of the condensate. Initially, we start with an equilibrium condensate profile for 104 atoms with a scattering length of $200a_0$. The scattering length is then instantaneously changed to $a = -3a_0$. The trap parameters are obtained from [43]. (b) Soliton train near the two turning points and near the center of oscillation.
Courtesy: Figures taken from [3, 43]

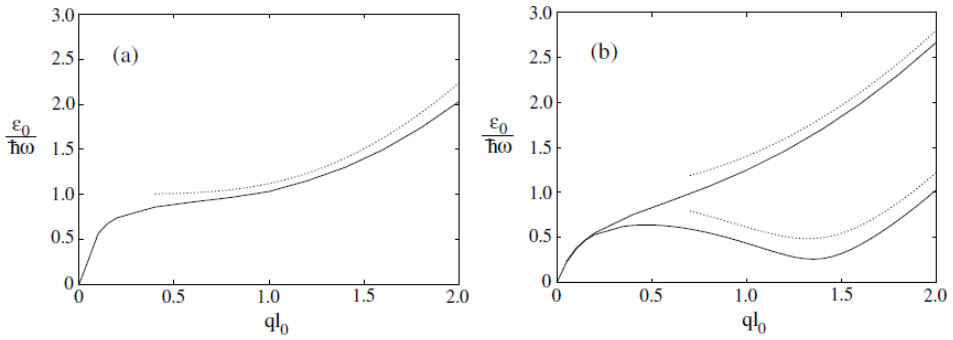

Figure 1.5: Dispersion law $\epsilon_0(q)$ for (a) $\beta = 0.5$, $\mu/\hbar\omega = 343$ and (b)$\beta = 0.53$, $\mu/\hbar\omega = 46$ (upper curve) and $\beta = 0.47$, $\mu/\hbar\omega = 54$ (lower curve). Here, $\beta = g/g_d$. Solid lines show numerical results, and dotted lines are the result of lowest branch of spectrum. We see the roton minimum in (b) at $q = (16\mu(1/2 - \beta)/15\hbar^2\omega^2 m)^{1/2}$.
Courtesy: Fig. taken from [39].

in purely dipolar gases. Dipole-dipole interactions (DDI) strongly influence the physics of the condensates and may completely change their properties. Two major characteristics of DDI are its long-range and anisotropic nature. These have important consequences on the properties of the condensate. Due to its long-range character, in the presence of DDI, all the partial waves contribute, contrary to the short-range interactions where it is dominated by only the s-wave.

An interesting feature of dipolar condensates is that they can exhibit a roton-maxon behaviour in the excitation spectrum which originates due to the momentum dependence of the interparticle interaction [39]. This behaviour was initially observed only in superfluid Helium and now such exhibition in trapped dipolar condensates brings interesting possibilities on manipulations of superfluid properties of trapped condensates. Fig. 1.5 shows the maxon- roton behaviour of a pancake-shaped dipolar condensates with dipoles aligned perpendicular to the trap plane.

The potential due to the dipole-dipole interaction is given by,

$$V_d(\mathbf{r}) = g_d \frac{1 - 3\cos^2\theta}{r^3} \tag{1.13}$$

where, $g_d = \dfrac{\gamma N d^2}{4\pi\epsilon_0}$ with γ being a tuning parameter, $\mathbf{r}$ is the radial vector between the two dipoles and θ is the angle between $\mathbf{r}$ and the dipole vector $\mathbf{d}$ as shown in Fig. 3.1(b). On including the DDI term, the non-linear GPE

takes the following form.

$$i\hbar\frac{\partial\psi(\mathbf{r},t)}{\partial t} = \left[\frac{-\hbar^2}{2m}\nabla^2 + V(\mathbf{r}) + g|\psi(\mathbf{r},t)|^2 + \int d\mathbf{r}' V_d(\mathbf{r}-\mathbf{r}')|\psi(\mathbf{r}',t)|^2\right]\psi(\mathbf{r},t) \quad (1.14)$$

The integral term in Eq. 1.14 introduces non-locality and non-linearity similar to that in nematic liquid crystals [34], and photorefractive screening solitons.

1.4 Tuning the Interaction Parameters

Tuning of g:
The short-range attraction parameter g can be tuned by changing the s- wave scattering length, a. This is achieved via a **Feshbach Resonance**, which arises when the short-range interaction energy between two atoms equals the energy of the bound state. This can be achieved by tuning the magnetic moments using a magnetic field leading to *magnetically tuned feshbach* and by optical methods resulting in an *optical feshbach*. The s- wave scattering length a as a function of the magnetic field B is as follows [10].

$$a(B) = a_{bg}\left(1 - \frac{\Delta}{B - B_0}\right) \quad (1.15)$$

where a_{bg} is the scattering length associated with the background potential V_{bg}, and Δ is the resonant width and B_0 is the resonance position where $a \to \pm\infty$. Fig. 1.6 shows the scattering length a and molecular state energy E near a magnetically tuned feshbach resonance.

Tuning of $\mathbf{g_d}$:
The dipolar interaction parameter g_d can be tuned by using the tuning parameter $\gamma = (3\cos^2\phi - 1)/2$, which can be changed from $-1/2$ to 1 by varying the angle ϕ between the z axis and the direction of dipole moment as shown in Fig. 1.7. This changes the dipolar interaction from attractive to repulsive, and at a particular angle, called the magic angle, $\alpha_m = 54.7°$, the dipolar interaction averages to zero [18].

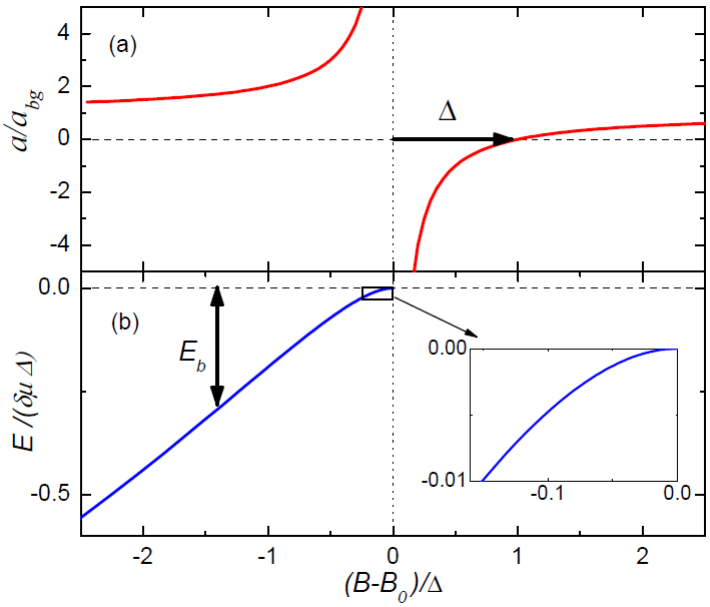

Figure 1.6: Scattering length a (Panel(a)) and molecular state energy E (Panel (b)) near a magnetically tunes Feshbach resonance. The binding energy is defined to be positive, $E_b = -E$. The inset shows the universal regime near the point of resonance where a is very large and positive.
Courtesy: Fig. taken from [10].

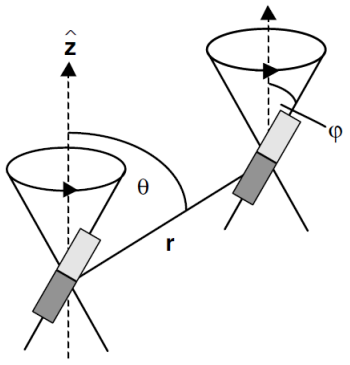

Figure 1.7: Tunability of the magnetic dipole interaction. Using time-varying magnetic fields, the dipoles are rapidly rotated around the z axis. The angle ϕ between the dipole orientation and the z axis determines the strength and sign of the effective interaction. $\phi = 0$: the magnetic dipoles are polarized along the z direction. $\phi = \pi/2$: the sign of the effective interaction is inverted and the absolute value is only half of the polarized case. $\phi = 54.7°$(magic angle): the dipolar interaction averages to zero.
Courtesy: Fig. taken from [18].

1.5 Overview

This thesis is organized as follows:

In chapter 2 we discuss two-dimensional bright solitons in dipolar BECs with dipoles aligned perpendicular [35], and parallel [44] to the 2D plane, summarizing the phonon instability and soliton stability conditions. We point out the difficulties in experimental observation of these solitons and hence the need to explore new configurations.

In chapter 3 we explore the case of two-dimensional bright solitons in dipolar BECs with tilted dipoles. We derive the condition for phonon instability, and show the crucial dependence of soliton stability on the tilting angle α. Lastly we discuss the stability regime for the specific cases of Chromium, Erbium and Dysprosium atoms.

In chapter 4 we give a summary of all the chapters.

Chapter 2

2D Bright Solitons in Dipolar BECs

Multi-dimensional solitons find many applications in the field of matter waves and nonlinear optics. They have been experimentally observed in nematic liquid crystals [34] and in photorefractive solitons [40]. However, multidimensional solitons have not been observed in BECs with attractive short-range interactions as they are unstable against collapse. The nonlocality and the nonlinearity introduced by the dipolar interaction provides a possibility to stabilize two-dimensional bright solitons in dipolar BECs [35]. But so far there have been no reports of experimental observation of these solitons.

In this chapter we discuss 2D bright solitons in dipolar BECs, the theoretical work done so far on them and the experimental difficulties faced in finding them. So far, theorists have looked at two kinds of alignments of the dipoles w.r.t. to the 2D plane that contains them - dipoles aligned perpendicular to the 2D plane, and, parallel to it. The following sections describe both the cases briefly.

2.1 Dipoles Perpendicular to 2D Plane

This alignment was studied by Luis Santos and his group at Hannover in Germany [35]. The model consisted of a BEC of N particles confined to the xy 2D plane by a strong harmonic trap ω_z along the z axis, with their electric dipole d (also valid for magnetic dipole) pointing along the z axis (See Fig. 2.1). The solitons formed are isotropic with equal widths along the x and y directions, as seen in Fig. 2.2(a).

Considering the Gaussian ansatz for the wave function,

$$\psi(\bar{r}) = \frac{1}{\pi^{3/4} l_z^{3/2} L_\rho L_z^{1/2}} exp\left(-\frac{x^2+y^2}{2l_z^2 L_\rho^2} - \frac{z^2}{2l_z^2 L_z^2}\right),$$

where, $l_z = \sqrt{\frac{\hbar}{m\omega_z}}$ and L_ρ and, L_z are dimensionless parameters related to the Gaussian widths, the energy obtained was the following:

$$\frac{2E}{\hbar\omega_z} = \frac{1}{L_\rho^2} + \frac{1}{2L_z^2} + \frac{L_z^2}{2} + \frac{1}{\sqrt{2\pi}L_\rho^2 L_z}\left[\frac{\tilde{g}}{4\pi} + \frac{\tilde{g_d}}{3} f\left(\frac{L_\rho}{L_z}\right)\right] \tag{2.1}$$

where,

$$\tilde{g}(\tilde{g_d}) = \frac{2}{\hbar\omega_z l_z^3} g(g_d)$$

$$f(\kappa) = \frac{1}{\kappa^2 - 1}\left[2\kappa^2 + 1 - \frac{3\kappa^2}{\sqrt{\kappa^2 - 1}} tan^{-1}\sqrt{\kappa^2 - 1}\right]$$

with $\kappa = L_\rho / L_z$. From inspection, we see that the energy has a minimum in L_ρ if

$$\frac{\tilde{g_d}}{3\sqrt{2\pi}} < 1 + \frac{\tilde{g}}{2(2\pi)^{3/2}} < \frac{-2\tilde{g_d}}{3\sqrt{2\pi}}$$

This happens only when $g_d < 0$ (g_d can be made negative with the help of rotating fields as discussed in Section 1.7) and the ratio $\beta = \frac{g_d}{g}$ is such that

$$|\beta| > \frac{3}{8\pi} \sim 0.12 \tag{2.2}$$

Thus 2D bright solitons can be found in dipolar BECs with dipoles aligned perpendicular to the 2D plane only when the DDI term $g_d < 0$ and the ratio $|\beta| > 0.12$.

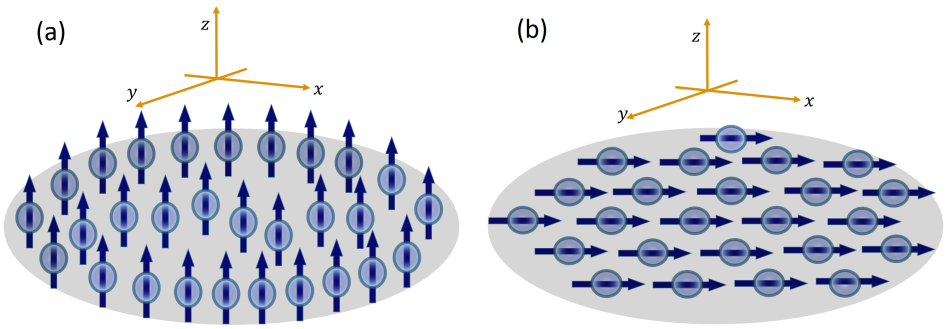

Figure 2.1: Schematic setup of dipolar BEC in the xy plane with strong harmonic trap along z axis with dipoles aligned (a) perpendicular to the 2D plane, and , (b) parallel to the 2D plane.

2.2 Dipoles Parallel to 2D Plane

This case was studied by a group in Israel [44] where the model was similar to the case discussed in section 2.1, only the dipoles were aligned parallel to the 2D plane containing the BEC (as shown in Fig. 2.1). This arrangement

makes the DDI anisotropic in the 2D plane. This is seen in Fig. 2.2(b) where the soliton is elongated along the x axis.

Considering the following Gaussian ansatz,

$$\psi(\bar{r}) = \frac{1}{\pi^{3/4} l_x^{1/2} l_y^{1/2} l_z^{1/2}} exp\left(-\frac{x^2}{2l_x^2} - \frac{y^2}{2l_y^2} - \frac{z^2}{2l_z^2}\right),$$

the following energy is obtained:

$$E = \frac{1}{4}\left(\frac{1}{l_x^2} + \frac{1}{l_y^2} + \frac{1}{l_z^2}\right) + \frac{l_z^2}{4} + \frac{1}{\sqrt{2\pi} l_x l_y l_z}\left[\frac{g}{4\pi} + \frac{g_d}{3} h(\kappa_x, \kappa_y)\right] \quad (2.3)$$

where,

$$\kappa_{x(y)} = \frac{l_{x(y)}}{l_z}$$

$$h(\kappa_x, \kappa_y) = \int_0^1 \frac{3x^2 \kappa_x \kappa_y dx}{\sqrt{1 + (\kappa_x^2 - 1)x^2}\sqrt{1 + (\kappa_y^2 - 1)x^2}} - 1$$

Investigating this energy expression, we see that there exists a minimum only when $g_d > 0$ and,

$$\beta = \frac{g_d}{g} > \frac{3}{4\pi} \sim 0.24 \quad (2.4)$$

Thus 2D bright solitons can be found in dipolar BECs with dipoles aligned parallel to the 2D plane when the DDI term $g_d > 0$ and the ratio $\beta > 0.24$.

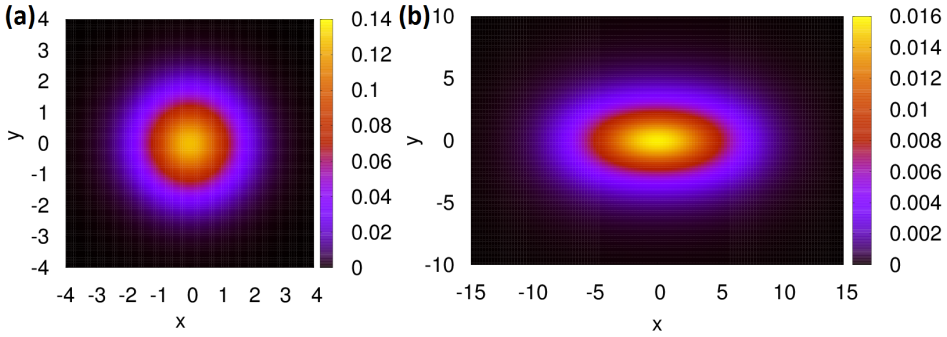

Figure 2.2: Condensate density $|\psi|^2$ for the ground state of a 2D bright soliton with $\tilde{g} = 20$ and $|\beta| = 0.4$ for (a) isotropic perpendicular case (b) anisotropic parallel case, obtained from numerical solutions of the GPE. *Courtesy:* These plots have been borrowed from Chinmayee Mishra.

2.3 Phonon Instability and the Gas of Solitons

The partially attractive behavior of the DDI leads to phonon instability (PI) in dipolar BECs. In 2D dipolar BECs, post PI dynamics results in the transient formation a gas of attractive, inelastic 2D bright solitons that eventually fuse into a larger bright soliton. This is in contrast to 2D and 3D BECs with only short-range interactions, where the condensates just collapse [38].

Consider the 2D homogenous solution of Eq. 1.5:

$$\psi_{2D}(\mathbf{r},t) = \sqrt{n_{2D}} exp\left(\frac{-i\mu_{2D}t}{\hbar}\right)$$

where n_{2D} is the homogenous 2D density and μ_{2D} is the 2D chemical potential. Solving for μ_{2D} from the GPE 1.5, we get the following expressions in the perpendicular and the parallel cases respectively.

$$\begin{aligned} \mu_{2D(\perp)} &= \frac{gn_{2D}}{\sqrt{2\pi}l_z}\left(1+\frac{8\pi\beta}{3}\right) \\ \mu_{2D(\parallel)} &= \frac{gn_{2D}}{\sqrt{2\pi}l_z}\left(1-\frac{4\pi\beta}{3}\right) \end{aligned} \tag{2.5}$$

When $\mu < 0$, the Bogoliubov excitations, $\epsilon(\kappa \to 0) \sim \sqrt{\mu}\kappa$ are purely imaginary resulting in phonon instability. Thus, setting $\mu < 0$ in Eqs. 2.5, we obtain the condition for PI are the following:

$$\begin{aligned} \perp \text{case} : \beta &< -\frac{3}{8\pi} \\ \parallel \text{case} : \beta &> \frac{3}{4\pi} \end{aligned} \tag{2.6}$$

We note that the conditions for the formation of stable solitons 2.2 and 2.4 are the same as the conditions for phonon instability 2.6. The fact that these two conditions are identical is not accidental, but it shows that post phonon instability dynamics may lead to the formation of bright solitons. The following Fig. 2.3 shows the formation of 2D soliton gas after phonon instability.

2.4 Experimental Difficulties

As discussed earlier in section 2.1, we require $g_d < 0$ for the formation of 2D bright solitons in dipolar BECs with perpendicular dipoles. The DDI parameter g_d can be made negative by changing the tuning parameter γ. However, this seems impossible to be achieved experimentally. In the parallel configuration, the regime for stability of the 2D bright solitons in the parameter space is extremely small, again making it difficult to produce them experimentally. Thus so far, there have been no reports of experimental production

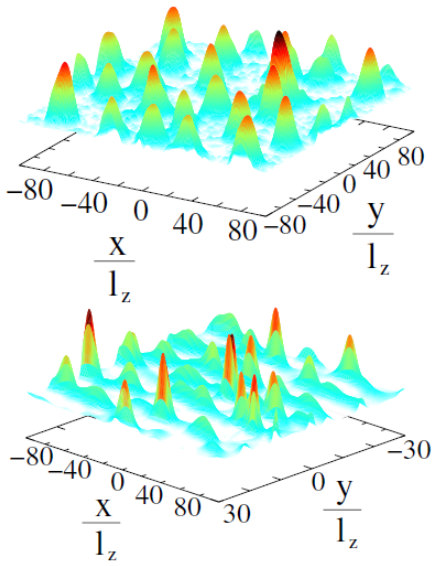

Figure 2.3: The 2D soliton gas after phonon instability of a homogeneous dipolar BEC with $\mu = -0.2$ and $g/(\sqrt{2\pi}l_z) = 10$. (top) $\perp$- configuration, $\beta = -0.2$, $t = 484/\omega_z$; (bottom) $\|$- configuration, $\beta = 0.3$, and $t = 108/\omega_z$. *Courtesy:* Fig. taken from [38]

of 2D bright solitons in dipolar BECs.

In this thesis we alter the configuration of the system by tilting the dipoles at an angle α w.r.t the z axis. As we shall show, this gives a better control of the system and helps in tuning of the interaction parameters, which is crucial in the experimental achievement of 2D bright solitons.

2.5 Summary

In this chapter we discussed the properties of 2D bright solitons in a dipolar BEC with dipoles aligned in the two different configurations - perpendicular and parallel, focusing on phonon instability and the stability regions of the solitons. We also discussed the difficulties faced in the experimental realizations of these solitons and hence the need to explore new configurations in order to observe them experimentally.

Chapter 3

2D Bright solitons in Dipolar BECs with Tilted dipoles

3.1 Setup and Model

We consider a dipolar BEC containing N atoms with mass m and electric or magnetic dipolar moment d oriented in the xz plane making an angle α w.r.t. the z axis using external magnetic fields as shown in Fig. 3.1. Since we are interested in 2D self- trapped solutions of the GPE, we consider no external traps in the xy plane and a sufficiently strong trap along the z direction given by $V_{ext}(\mathbf{r}) = m\omega_z^2/2$ in order to hold the condensate in the 2D plane.

The atoms interact amongst each other via two kinds of interactions: (i) Short-range contact interaction: we consider repulsive short-range interaction between the atoms of the condensate characterized by a positive s - wave scattering length a. The coupling constant for the interaction is given by $g = 4\pi\hbar^2 aN/m$. (ii) Long-range dipole-dipole interaction (DDI): the atoms interact via the dipole -dipole potential: $V_d(\mathbf{r}) = g_d(1 - 3\cos^2\theta)/r^3$, where $\mathbf{r}$ is the radial vector joining the two dipoles, θ is the angle between $\mathbf{r}$ and $\mathbf{d}$, and, $g_d = \gamma d^2$ is the strength of the dipole-potential with γ being a parameter tunable using rotating fields [18].

3.1.1 Model: Reduced 2D GPE

We closely follow the methods illustrated in [35]. At sufficiently low temperatures, we can describe the above system using the following non-local, non-linear Schödinger equation (NLGPE):

$$\begin{aligned} i\hbar\frac{\partial\Psi(\mathbf{r},t)}{\partial t} &= \Bigg[-\frac{\hbar^2}{2m}\nabla^2 + V_{ext}(\mathbf{r}) + g|\Psi(\mathbf{r},t)|^2 \\ &\quad + \int d\mathbf{r}' V_d(\mathbf{r}-\mathbf{r}')|\Psi(\mathbf{r}',\mathbf{t})|^2\Bigg]\Psi(\mathbf{r},t) \end{aligned} \tag{3.1}$$

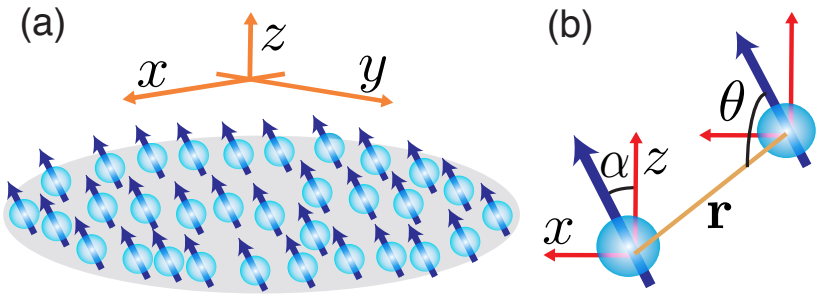

Figure 3.1: (a) Schematic setup of dipolar BEC in the xy plane with strong harmonic trap along z axis. (b) Dipoles aligned in the xz plane making an angle α with the z axis and angle θ between the radial vector $\mathbf{r}$ and the dipole moment $\mathbf{d}$.

where $\Psi(\mathbf{r},t)$, normalized to unity by $\int d\mathbf{r}|\Psi(\mathbf{r},t)|^2 = 1$, is the BEC wave function. Since there is a strong trap along the z axis and the condensate lies on the xy 2D plane, we can factorize $\Psi(\mathbf{r})$ as $\Psi(\mathbf{r}) = \psi(x,y)\phi_0(z)$. We consider the trapping such that the system is frozen in the ground state of the harmonic oscillator along the z axis, given by $\phi_0 = \frac{1}{\pi^{1/4}l_z^{1/2}}e^{-z^2/2l_z^2}$, where $l_z = \sqrt{\frac{\hbar}{m\omega_z}}$. Using Fourier transform of the dipole potential and convolution theorem, and by multiplying Eq. 3.1 with $\phi_0^*(0)$ and integrating over dz and dk_z we obtain the following quasi-2D NLGPE:

$$i\hbar\frac{\partial\psi(x,y,t)}{\partial t} = \Big[-\frac{\hbar^2}{2m}\nabla_{x,y}^2 + \frac{g}{\sqrt{2\pi}l_z}|\psi(x,y,t)|^2 + \frac{2g_d}{3l_z} \times \int \frac{d^2k}{(2\pi)^2}e^{i(k_x x+k_y y)}f(k_\rho l_z)\tilde{n}(k_x,k_y)\Big]\psi(x,y,t) \quad (3.2)$$

where $\tilde{n}(k_x,k_y)$ is the Fourier transform of the 2D condensate density $|\psi(x,y)|^2$ with $k_\rho^2 = k_x^2 + k_y^2$ and the function,

$$f(k) = \sqrt{2\pi}(3\cos^2\alpha - 1) + 3\pi e^{k^2/2}\mathrm{Erfc}\left(\frac{k}{\sqrt{2}}\right) \times(\sin^2\alpha\cos^2\theta_k - \cos^2\alpha) \quad (3.3)$$

where $\mathrm{Erfc}(x)$ is the complimentary error function, and $k_x = k_\rho\cos\theta_k$. Using the reduced 2D NLGP Eq. 3.2 we study the formation and dynamics of 2D bright solitons in the following sections.

3.2 Bogoliubov Excitations in a 2D Homogeneous BEC

In this section we calculate the Bogoliubov excitations for our system for which we first calculate the chemical potential μ_{2D}. The time-dependent homogeneous solution of Eq. 3.2 is given by $\psi(x,y,t) = \sqrt{n_{2D}}e^{-i\mu_{2D}t/\hbar}$ where n_{2D} is the homogeneous density and μ_{2D} is the 2D chemical potential. Substituting this into Eq. 3.2 and solving for the 2D chemical potential we obtain:

$$\mu_{2D} = \frac{gn_{2D}}{\sqrt{2\pi}l_z}\left[1+\frac{4\pi}{3}\beta(3\cos^2\alpha-1)\right] \tag{3.4}$$

where $\beta = \frac{g_d}{|g|}$ determines the relative strength between short- range contact interaction and the long-range dipolar interaction. We then calculate the elementary excitations of the above homogeneous solution using the method illustrated in Section 1.1.2. They are of the following form:

$$\delta\psi(x,y,t) = u_0 e^{-i(\mathbf{k}.\rho-\omega_{\mathbf{k}}\mathbf{t})} + v_0 e^{i(\mathbf{k}.\rho-\omega_{\mathbf{k}}\mathbf{t})} \tag{3.5}$$

with the dispersion given by,

$$\epsilon_{\mathbf{k}} = \hbar\omega_{\mathbf{k}} = \sqrt{E_k\left[E_k+\frac{2gn_{2D}}{\sqrt{2\pi}l_z}\left(1+\frac{2\sqrt{2\pi}}{3}\beta f(k)\right)\right]} \tag{3.6}$$

where $E_k = \hbar^2(k_x^2+k_y^2)/2m$.

3.2.1 Phonon Instability and Soliton Formation

As seen from Eq. 3.6, the phonon modes $\epsilon(k\to 0) \simeq \sqrt{\mu}k$ become imaginary (and hence unstable) when $\mu < 0$ which gives us the following condition for phonon instability (PI).

$$g < -\frac{4\pi g_d}{3}\left(3\cos^2\alpha-1\right) \tag{3.7}$$

or,

$$|\beta| > \frac{3}{4\pi|3\cos^2\alpha-1|} \tag{3.8}$$

We note that setting $\alpha = 0$ $(\pi/2)$ reduces to the perpendicular (parallel) configuration giving the phonon instability condition $|\beta| > 0.12$ (0.24) as discussed in Section 2.3.

Fig. 3.2 shows the phonon instability regions as a function of β and α in the two different scenarios (a) $g > 0$ and (b) $g < 0$. We shall focus on only the former case ($g > 0$) as in the latter case, PI always leads to instability of the condensate against local collapses similar to 2D non-dipolar BEC with short-range interactions. When $g > 0$ post PI dynamics is characterized by

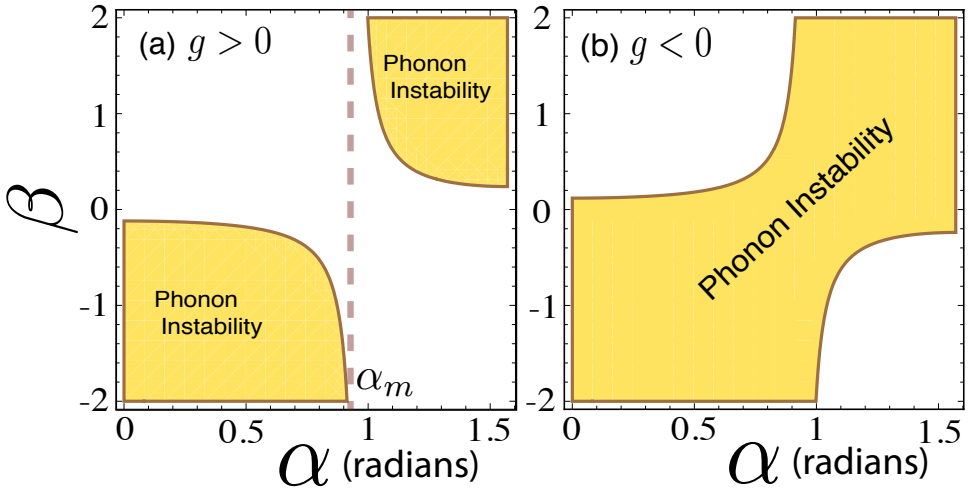

Figure 3.2: Phonon instability regions (shaded) as a function β and tilting angle α for (a) g>0 and (b) g<0. Dashed line in Fig. 3.2 (a) indicates the magic angle α_m across which dipolar characteristics need to be reversed for stable solitons. In the former case post PI dynamics is characterized by the formation of 2D solitons, while in the latter case the BEC becomes unstable against local collapses.

the formation of 2D bright soliton gas, if $\mu_{2D} \ll \hbar\omega_z$ [38].

The phonon instability region as a function of β and α with g>0 (Fig. 3.2a) gives us the first estimate for the stability regions of the 2D bright solitons. As is clear from Fig. 3.2(a), there exist two islands of stable regions separated at the magic angle $\alpha_m = 54.7°$ (0.95 radians) below which we need $g_d < 0$ and above which we need $g_d > 0$ for the formation of stable bright solitons.

We note that sufficiently increasing the strength of dipolar interaction g_d, the condensate tends to enter the collapse instability region. This gives us the upper cut- off for $|\beta|$ in the PI region for the stability of solitons which we estimate using Gaussian variational calculations in the following section.

3.3 Gaussian Calculations

In this section, we analyze the stability of 2D bright solitons in a dipolar BEC with tilted dipoles using a three- dimensional variational analysis. We consider the following Gaussian-like ansatz to determine the stability regime of 2D bright solitons as a function of the parameters g, g_d, and, α.

$$\Psi(\mathbf{r}) = \frac{1}{\pi^{3/4} l_z^{3/2} \sqrt{L_x L_y L_z}} exp\left[-\frac{1}{2l_z^2}\left(\frac{x^2}{L_x^2} + \frac{y^2}{L_y^2} + \frac{z^2}{L_z^2}\right)\right] \tag{3.9}$$

Here, L_x, L_y and L_z are dimensionless parameters related to the widths of the Gaussian along x, y and z directions respectively, and $l_z = \sqrt{\frac{\hbar}{m\omega_z}}$ as

mentioned previously in section 3.1.1. The Gaussian analysis well captures the two boundaries of the stability regime: (a) Expansion instability: the repulsive nature due to g dominates over the attraction due to g_d making the solitons unstable against 2D expansion, and, (b) Collapse instability: attractive interaction due to g_d dominates repulsive interaction due to g resulting in a 3D collapse.

3.3.1 Energy of the System

The energy of the system is obtained by using the above Gaussian ansatz 3.9 for the condensate wave function in the following energy expression:

$$\begin{aligned} E &= \int d\mathbf{r}\left[\frac{\hbar^2}{2m}|\nabla\Psi(\mathbf{r})|^2 + V_{ext}(\mathbf{r})|\Psi(\mathbf{r})|^2 + \frac{g}{2}|\Psi(\mathbf{r})|^4\right] \\ &\quad + \frac{1}{2}\int d^3\mathbf{r}'\, V_d(\mathbf{r}-\mathbf{r}')\,|\Psi(\mathbf{r})|^2\,|\Psi(\mathbf{r}')|^2 \end{aligned} \tag{3.10}$$

The last term in the energy functional describes the non-local, nonlinear dipolar interaction, which can be evaluated with the help of Fourier transformation and convolution theorem, and thus simplifying to

$$\int d\mathbf{r}\int d\mathbf{r}'\, V_d(\mathbf{r}-\mathbf{r}')\,|\Psi(\mathbf{r})|^2\,|\Psi(\mathbf{r}')|^2 = \int \frac{d\mathbf{k}}{(2\pi)^3}\tilde{V}_d(\mathbf{k})\tilde{n}_0^2(\mathbf{k}) \tag{3.11}$$

where,

$$\begin{aligned} \tilde{V}_d(k) &= \frac{4\pi}{3}g_d(3\cos^2\theta - 1) \\ &= \frac{4\pi}{3}g_d\left[\frac{3(k_\rho^2\cos^2\theta\sin^2\alpha + k_\rho k_z\cos\theta\sin 2\alpha + k_z^2\cos^2\alpha)}{k_\rho^2 + k_z^2} - 1\right] \end{aligned} \tag{3.12}$$

and,

$$\tilde{n}(\mathbf{k}) = \exp\left[-\frac{l_z^2}{2}\left(k_x^2L_x^2 + k_y^2L_y^2 + k_z^2L_z^2\right)\right] \tag{3.13}$$

After simplifying the integrals, and scaling the interaction parameters as $\tilde{g}(\tilde{g}_d) = g(g_d)/\sqrt{2\pi}\hbar\omega_z l_z^3$, we thus arrive at the final expression for the energy of our system.

$$\begin{aligned} \frac{E}{\hbar\omega_z} &= \frac{1}{4L_x^2} + \frac{1}{4L_y^2} + \frac{1}{4L_z^2} + \frac{L_z^2}{4} + \frac{1}{L_xL_yL_z}\frac{\tilde{g}}{4\pi} \\ &+ \frac{\tilde{g}_d}{3L_z}\left[\frac{-1}{L_xL_y} + \frac{3\cos^2\alpha}{\sqrt{(L_x^2-L_z^2)(L_y^2-L_z^2)}} - \frac{3\sin^2\alpha}{L_x^2-L_y^2}\left(\frac{L_y}{L_x} - \sqrt{\frac{L_y^2-L_z^2}{L_x^2-L_z^2}}\right)\right] \\ &+ \frac{\tilde{g}_d}{2\pi}\int_0^{2\pi} d\theta \frac{\cos^2\theta\sin^2\alpha - \cos^2\alpha}{(\cos^2\theta L_x^2 + \sin^2\theta L_y^2 - L_z^2)^{3/2}} \\ &\qquad \times tan^{-1}\left(\frac{\sqrt{\cos^2\theta L_x^2 + \sin^2\theta L_y^2 - L_z^2}}{L_z}\right) \end{aligned} \tag{3.14}$$

(Derivation of the DDI term is shown in details in Appendix B.1). Putting $\alpha = 0$ and $\alpha = \pi/2$ reduces the energy expression for the perpendicular (Eq. 2.1) and parallel (Eq. 2.3) configurations respectively. The following Fig. 3.3 shows equal energy surfaces around the local minimum of the energy 3.14 as a function of the variational parameters L_x, L_y and L_z.

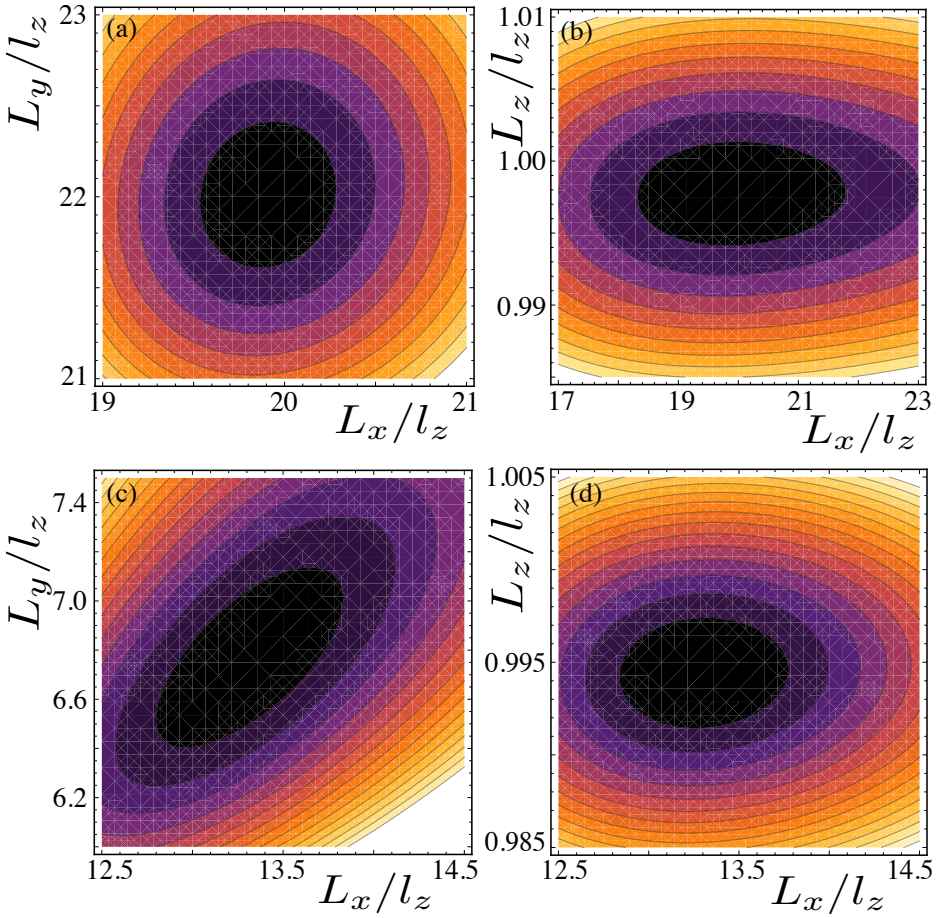

Figure 3.3: Equi-energy surfaces around the local minimum of the energy 3.14 as a function of variational parameters L_x, L_y and L_z. The centre of the inner (black) surface gives the equilibrium widths $\{w_x^0, w_y^0, w_z^0\}$ of the bright soliton. The plots (a) and (b) are for $\tilde{g} = 100, \beta = -0.2$ and $\alpha = 0.42$ radians with $\{w_x^0, w_y^0, w_z^0\} \to \{19.9, 22, 0.997\}$, and, the plots (c) and (d) correspond to $\tilde{g} = 20, \beta = 0.5$ and $\alpha = 1.3$ radians with $\{w_x^0, w_y^0, w_z^0\} \to \{13.3, 6.7, 0.99\}$

3.3.2 Stability Regime

In order to obtain the stability regime, we minimize the energy functional 3.14 w.r.t. the Gaussian widths L_x, L_y and L_z. Since the energy involves an integral term that is not solvable analytically, we use numerical methods for minimization. Depending on the values of the parameters g, g_d and α, the

minimum may or may not exist. The existence of a minimum in the energy functional suggests the stability of the bright solitons. Fig. 3.4 shows the regions in the $g-g_d-\alpha$ parameter space where stable solitons can be formed. As is seen in the figure, this regime for $\alpha = \pi/2$ is very small as compared to $\alpha = 0$, consistent with the discussion in Section 2.4.This is in general true and not just for $\alpha = 0$ and $\pi/2$. The stability regime for $\alpha > \alpha_m$ is much smaller compared to that for $\alpha < \alpha_m$. We also note that by increasing the tuning angle α from 0 to α_m, we increase the region of stable solitons in the $g - gd$ phase space. Similarly, increasing α from α_m to $\pi/2$, increases the stability regime.

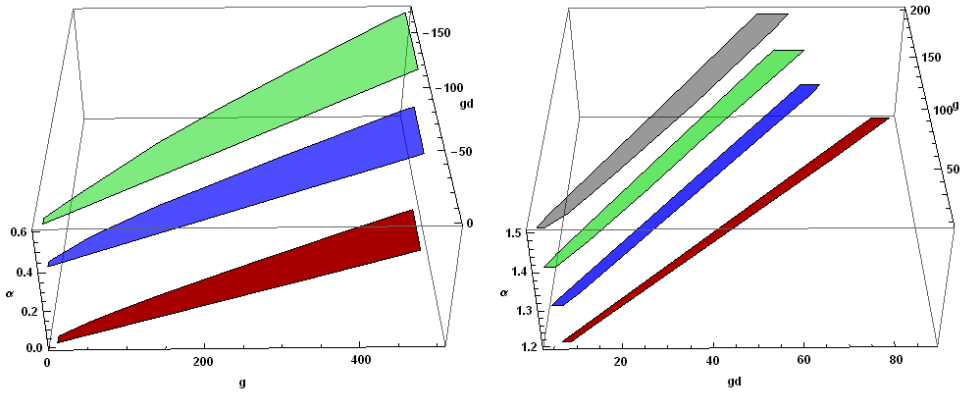

Figure 3.4: Regions for the formation of stable soliton (coloured) in the $g - g_d - \alpha$ phase space for (a) $\alpha < \alpha_m$ and (b) $\alpha > \alpha_m$. The regions have been obtained for $\alpha = 0$ (red), 0.4 (blue), and 0.6 (green) in Fig 3.4(a), and $\alpha = 1.2$ (red), 1.3 (blue), 1.4 (green) and 1.5(grey) in Fig.3.4(b)

3.3.3 Anisotropic Solitons

When the dipoles are aligned perpendicular to the 2D xy plane ($\alpha = 0$), the solitons are isotropic and the Gaussian solution has equal widths $L_x = L_y$. However, tilting the dipoles towards the x-direction, causes the DDI in the xy plane to behave anisotropically, becoming partially repulsive and partially attractive. When $\alpha > \alpha_m$, this is characterized by $L_x > L_y$ (the condensate is elongated along the x axis), and when $\alpha < \alpha_m$, we have $L_x < L_y$ (the condensate is elongated along the y-axis), thus giving rise to anisotropic solitons. This can be seen in Fig. 3.5, which shows the density plots for the ground state of the bright solitons for different α values. On increasing α, the anisotropic behaviour increases, and as seen in Fig. 3.6, maximum anisotropy is exhibited when the dipoles are aligned parallel to the 2D plane ($\alpha = \pi/2$). We also see that anisotropy increases with increase in $|g_d|$, keeping g fixed, (see Fig. 3.6 (a),(c)) and, with increase in g keeping g_d fixed (Fig. 3.6 (b),(d)).

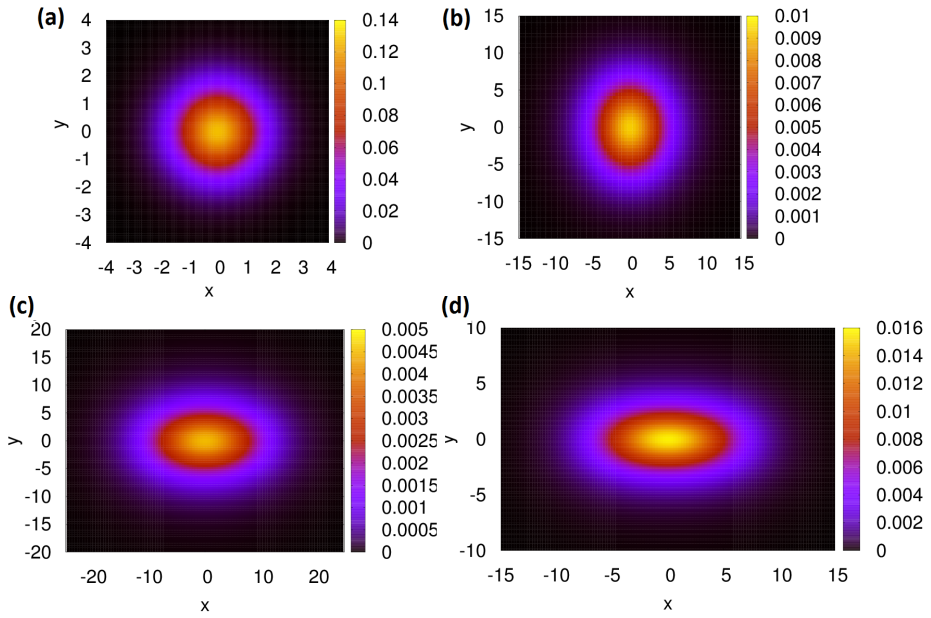

Figure 3.5: Condensate density $|\psi|^2$ plots for the ground state of a 2D bright soliton by numerical solutions of the GPE for $\tilde{g} = 20$, $|\beta| = 0.4$ and (a) $\alpha = 0$, (b) $\alpha = 0.6$, (c) $\alpha = 1.4$, (d) $\alpha = \pi/2$. The soliton is isotropic for $\alpha = 0$ and maximally anisotropic for $\alpha = \pi/2$.
Courtesy: These plots have been borrowed from Chinmayee Mishra.

To quantify the in-plane anisotropy, we define the ratio $\gamma = w_i^0/w_j^0$ in the xy plane where $i, j \in x, y$ with $w_j^0 > w_i^0$ so that γ is always less than unity. Thus for the $\alpha < \alpha_m$ region where $\beta < 0$ we have $\gamma = w_x^0/w_y^0$, since the soliton is more elongated along the y-axis (see Fig. 3.6a), and in the $\alpha > \alpha_m$ region where $\beta > 0$, we get $\gamma = w_y^0/w_x^0$ (see Fig. 3.6b). We discuss the two cases: (a) $\beta < 0 (0 \leq \alpha < \alpha_m)$ and (b) $\beta > 0 (\alpha_m < \alpha \leq \pi/2)$ separately and the results are shown in Figs. 3.6 c-f.

When $\beta < 0$, increasing α from 0 to α_m has two effects: (i) the soliton becomes anisotropic with $w_y^0 > w_x^0$ since DDI is more attractive along the y direction compared to x and, (ii) both w_x^0 and w_y^0 increase monotonously with α since the effective attractive interaction in the condensate is reduced. Interestingly, $\gamma = w_x^0/w_y^0$ as a function of α shows a non-monotonous behaviour leading to a local minimum, i.e., as α increases the anisotropy of the soliton increases (the ratio γ decreases), and surprisingly close to the expansion instability we observe a healing processes, the anisotropic character starts to diminish, before it becomes unstable against 2D expansion if $\alpha \geq \alpha_c (< \alpha_m)$, a critical angle determined by the explicit values of interaction parameters g and g_d. Each curves in Figs. 3.6c-d terminates on the point at which the soliton becomes unstable against expansion.

When $\pi/2$, the dipoles are aligned along the x axis, we get maximally anisotropic solitons for a fixed g and g_d (see Figs. 3.6e-f). Such a soliton is more prone to collapse instability with a slight increase in DDI. As shown in Figs. 3.6e-f, the anisotropy of the soliton can be reduced by simply tilting the dipoles out of the 2D plane, which may enhance the stability of the solitons, and involves no additional complications to the current experimental setups.

3.4 Variational Calculations

In this section we calculate the lowest- lying modes of our system using the Lagrangian formalism [45]. This helps us to understand better, the stability and dynamics of the 2D solitary waves. The Lagrangian density of our system is as follows

$$\begin{aligned} \mathcal{L} &= \frac{i}{2}\hbar\left(\psi\frac{\partial\psi^*}{\partial t} - \psi^*\frac{\partial\psi}{\partial t}\right) + \frac{\hbar}{2m}|\nabla\psi|^2 + V_{ext}(r)|\psi|^2 + \frac{g}{2}|\psi|^4 \\ &\quad + \frac{1}{2}|\psi|^2\int dr' V_d(r-r')|\psi(r')|^2 \end{aligned} \tag{3.15}$$

We consider the following time-dependent Gaussian like solution

$$\psi(x,y,z,t) = A(t)\prod_{\eta=x,y,z} e^{-\frac{(\eta-\eta_0(t))^2}{2w_\eta^2(t)}} e^{i(\eta\alpha_\eta(t)+\eta^2\beta_\eta(t))} \tag{3.16}$$

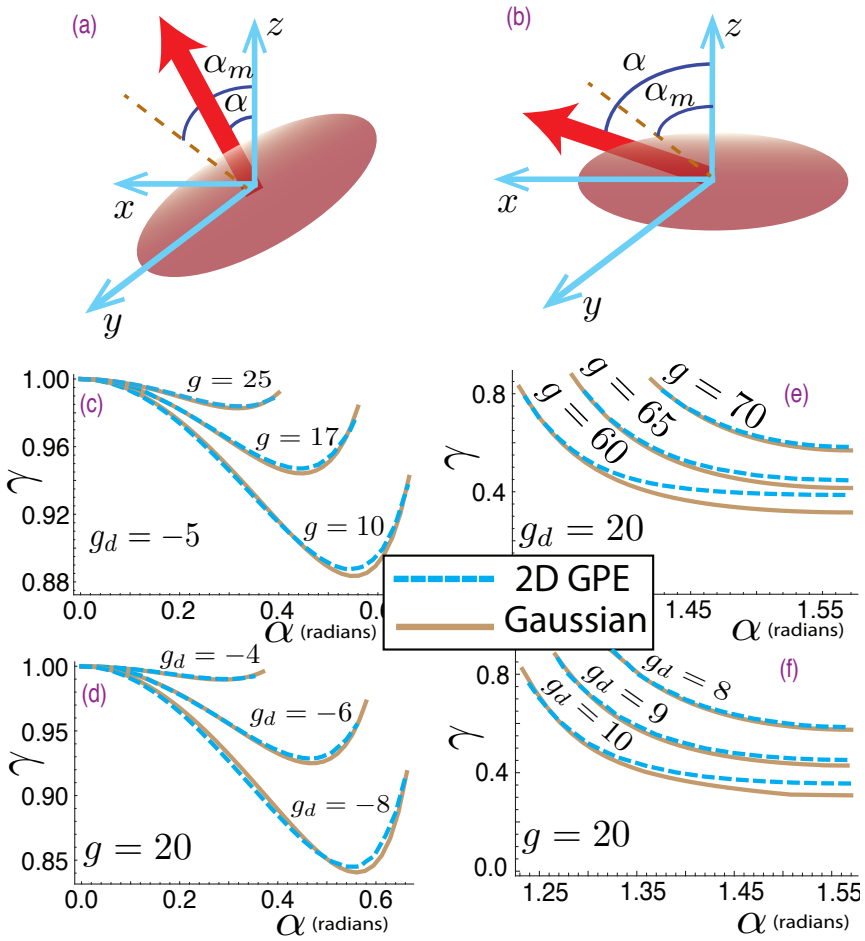

Figure 3.6: Equilibrium structure of the soliton for (a) $\beta < 0$ ($0 \leq \alpha \leq \alpha_m$) and (b) $\beta > 0$ ($\alpha_m <\leq \pi/2$). The thick (red) arrow shows the orientation of the dipoles in the system. For the case (a) the soliton is more elongated in along the y axis and hence the ratio $\gamma = w_x^0/w_y^0$. γ as a function of α for case (a) is shown in (c) for fixed g_d with different g values and vice versa in (d). The point at which each curves terminates marks the expansion instability of the soliton. For case (b) the soliton is more elongated along the x axis, and hence we define $\gamma = w_y^0/w_x^0$, and the corresponding plots as a function of α are shown in (e) and (f). In this case the starting points for the curves mark the stability against expansion.

where η_0 (center of the condensate), w_η (width), α_η (the slope), β_η (curvature radius $^{-1/2}$) are the time-dependent variational parameters. We aim to find the equations of motion governing the evolution of these parameters. For this, we first calculate the Lagrangian by integrating the Lagrangian density over all space

$$L = \langle \mathcal{L} \rangle = \int d\mathbf{r}\mathcal{L} \tag{3.17}$$

and hence obtaining,

$$\begin{aligned} L &= \hbar \sum_{x,y,z} \left[\left(\frac{\dot{\beta}_\eta w_\eta^2}{2} \right) + \dot{\alpha}_\eta \eta_0 + \dot{\beta}_\eta \eta_0^2 \right] + \frac{\hbar^2}{2m} \sum_\eta \left[\left(\frac{1}{2w_\eta^2} + \alpha_\eta^2 + 2\beta_\eta^2 w_\eta^2 \right) \right. \\ &\left. + 4\alpha_\eta \beta_\eta \eta_0 + 4\beta_\eta^2 \eta_0^2 \right] + \frac{1}{2} m\omega_z^2 \left(\frac{w_z^2}{2} + z_0^2 \right) + \frac{g}{\sqrt{2\pi}} \frac{1}{4\pi w_x w_y w_z} \\ &+ \frac{g_d}{12\pi^2} \int dk (3\cos^2\theta_{k.d} - 1) \prod_{\eta=x,y,z} e^{-\frac{k_\eta^2 w_\eta^2}{2}} \end{aligned} \tag{3.18}$$

We now solve the Euler-Lagrange equations for the parameters.

$$\frac{d}{dt}\frac{\partial L}{\partial \dot{q}_j} - \frac{\partial L}{\partial q_j} = 0 \tag{3.19}$$

where $q_j \equiv (x_0, y_0, z_0, w_x, w_y, w_z, \alpha_x, \alpha_y, \alpha_z, \beta_x, \beta_y, \beta_z)$.

3.4.1 Equations of Motion

Solving 3.19 for α_η and β_η, we get

$$\beta_\eta = \frac{m\dot{w}_\eta}{2\hbar w_\eta} \tag{3.20}$$

$$\alpha_\eta = \frac{m}{\hbar}\left(\dot{\eta}_0 - \frac{\dot{w}_\eta \eta_0}{w_\eta} \right) \tag{3.21}$$

Next, we perform a gauge transform of the Lagrangian 3.18 to simplify the problem of elimination of the α and β. The following gauge transform leaves the action S invariant, preserving the equations of motion.

$$L' = L - \frac{dg}{dt} \tag{3.22}$$

where,

$$g = \hbar \sum_\eta \left[\alpha_\eta \eta_0 + \beta_\eta \left(\frac{w_\eta^2}{2} + \eta_0^2 \right) \right] \tag{3.23}$$

The new Lagrangian obtained is as follows

$$L' = \frac{-m}{2} \sum_\eta \left[\dot{\eta}_0^2 + \frac{\dot{w}_\eta^2}{2} - \frac{\hbar^2}{2m^2 w_\eta^2} \right] - \frac{m\dot{z}_0^2}{2} + \frac{1}{2} m\omega_z^2 \left(\frac{w_z^2}{2} + z_0^2 \right) \tag{3.24}$$

$$+ \frac{g}{2(2\pi)^{3/2} w_x w_y w_z} + \frac{g_d}{12\pi^2} \int dk (3\cos^2\theta_{k.d} - 1) \prod_{\eta=x,y,z} e^{-\frac{k_\eta^2 w_\eta^2}{2}} \tag{3.25}$$

Now solving for the equations of motion for w_η we get the following set of coupled integro- differential equations

$$m\ddot{w}_x = \frac{\hbar^2}{mw_x^3} + \frac{g}{(2\pi)^{3/2}w_x^2 x_y x_z} - 2\frac{\partial V}{\partial w_x} \tag{3.26}$$

$$m\ddot{w}_y = \frac{\hbar^2}{mw_y^3} + \frac{g}{(2\pi)^{3/2}w_x x_y^2 x_z} - 2\frac{\partial V}{\partial w_y} \tag{3.27}$$

$$m\ddot{w}_z = \frac{\hbar^2}{mw_z^3} - m\omega_z^2 w_z + \frac{g}{(2\pi)^{3/2}w_x x_y x_z^2} - 2\frac{\partial V}{\partial w_z} \tag{3.28}$$

where

$$V(w_x, w_y, w_z) = \frac{g_d}{12\pi^2}\int dk(3\cos^2\theta_{k.d} - 1)\prod_{\eta=x,y,z} e^{-\frac{k_\eta^2 w_\eta^2}{2}} \tag{3.29}$$

The above equations represent the a particle with coordinates (w_x, w_y, w_z) in the effective potential

$$\begin{aligned} U_{eff}(w_x, w_y, w_z) &= \frac{\hbar^2}{2m}\left(\frac{1}{w_x^2} + \frac{1}{w_y^2} + \frac{1}{w_z^2}\right) + \frac{m\omega_z^2 w_z^2}{2} \\ &\quad + \frac{g}{(2\pi)^{3/2}w_x w_y w_z} + V(w_x, w_y, w_z) \end{aligned} \tag{3.30}$$

The equilibrium condensate widths are then obtained by minimizing the effective potential U_{eff} 3.30 w.r.t. w_η.

3.4.2 Small Oscillations

To study small oscillations of the soliton, we find the frequencies of the three (a) normal, (b) breathing, and, (c) quadrupole modes by finding the eigenvalues of the second derivative (Hessian matrix) of the effective potential U_{eff} 3.30.

$$H = \begin{pmatrix} U_{w_x,w_x} & U_{w_x,w_y} & U_{w_x,w_z} \\ U_{w_y,w_x} & U_{w_y,w_y} & U_{w_y,w_z} \\ U_{w_z,w_x} & U_{w_z,w_y} & U_{w_z,w_z} \end{pmatrix} \tag{3.31}$$

where,

$$U_{w_\eta,w_{\eta'}} = \frac{\partial^2 U_{eff}}{\partial w_\eta \partial w_{\eta'}}$$

Since the Hessian matrix is symmetric, diagonalization gives us the frequency modes. We find the frequencies for the breathing and the quadrupole modes for a fixed g and α and plot them as a function of β in the following Fig. 3.7. This gives us the lower and upper cut-off of β in order to find stable solitons.

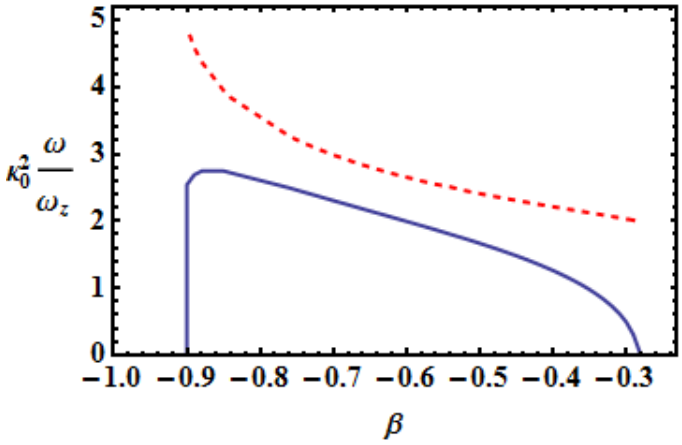

Figure 3.7: Breathing (blue solid) and quadrupole (red dashed) modes for $\tilde{g} = 20$, and $\alpha = 0.42$ with $\kappa_0 = L_\rho/L_z$

3.5 Calculations for Specific Atoms

In this section we calculate the region of stable solitons for specific cases of Chromium, Erbium and Dysprosium atoms. We consider condensates of $N = 10000$ atoms confined to the xy 2D plane by a harmonic trap of frequency $\omega_z = 2\pi$ kHz. We take the tuning parameter γ to be 1 in the positive β region and $-1/2$ in the negative β region. Using these values, we calculate the DDI parameter $\tilde{g}_d$ for the respective atoms using the following formula.

$$g_d = \frac{\gamma N \mu_0 m^2}{4\pi} \tag{3.32}$$

$$\tilde{g}_d = \frac{g_d}{\sqrt{2\pi} l_z^3 \hbar \omega_z} \tag{3.33}$$

where $\mu_0 = 4\pi \times 10^{-7}$ is the permeability of free space, m is the dipole moment of the atom ($= 6\mu_B$, $7\mu_B$ and $10\mu_B$ for Chromium, Erbium and Dysprosium respectively) and $l_z = \sqrt{\hbar/M\omega_z}$ with M being the mass of the atom ($= 52$ au, 167 au, and 162.5 au for Chromium, Erbium and Dysprosium respectively). This gives us the $\tilde{g}_d$ values of 21.763 for Chromium, 170.483 for Erbium and 333.956 for Dysprosium. We then find the region of stability of the bright solitons by spanning the $\alpha - \beta$ space. Fig. 3.8 shows the stable soliton regime in the $\alpha - \beta$ parameter space for a BEC of Chromium atoms. As consistent with our discussions in the previous sections, the regime for stability of solitons is very less in $\alpha > \alpha_m$ region as compared to the $\alpha < \alpha_m$ region.

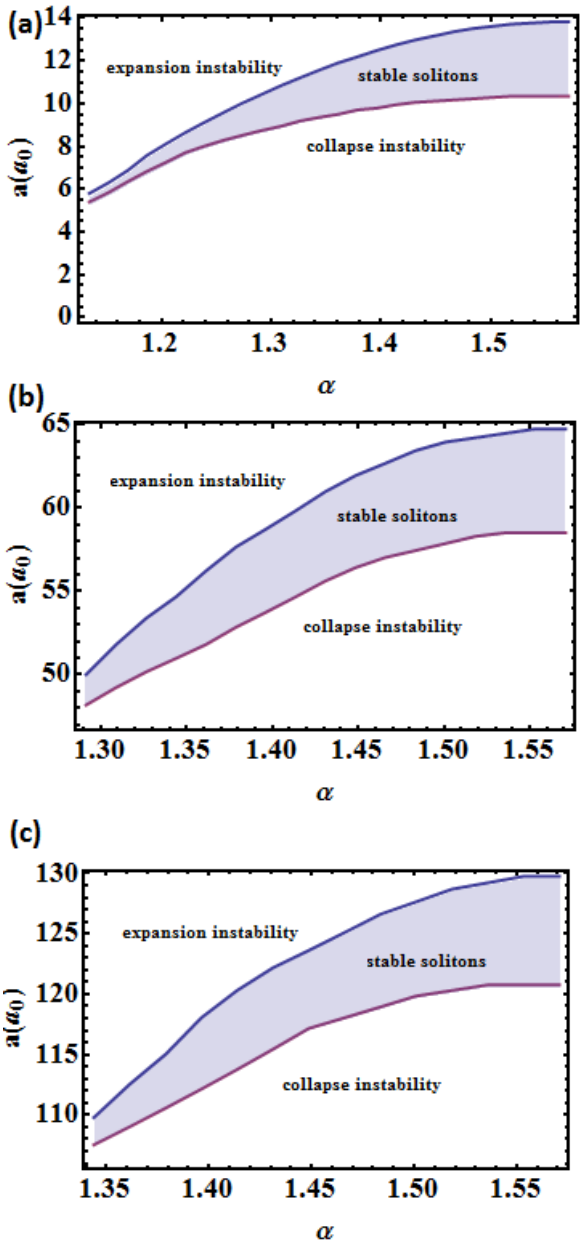

Figure 3.8: Plots showing the region of stable soliton in terms of the scattering length a (in Bohr radius a_0) and the tilting angle α for (a) chromium (b) erbium and (c)dysprosium atoms.

Chapter 4

Summary

In this thesis we have studied the physics of 2D bright solitons in dipolar BECs with tilted dipoles.

In chapter 1 we briefly introduced Bose- Einstein condensation and derived the Gross-Pitaevskii Equation which well captures the properties of BECs at very low temperatures. We then discussed about one-dimensional and multi-dimensional solitons in BECs with only self attracting interactions. Next, we learnt that dipolar interactions may stabilize multi-dimensional solitons in BECs.

In chapter 2 we discussed about two-dimensional solitons in the two different configurations, focusing on conditions of phonon instability which may lead to the formation of a gas of many solitons that merge to form a bigger soliton.

In chapter 3 we explored a new configuration by tilting the dipoles of the BEC. We first calculated the energy functional using variational method with Gaussian ansatz, and then obtained the stability regime in the $g - g_d$ phase for various α by minimizing the energy functional and looking for a local minimum. We saw that the region of stable solitons increases with increase in α in the two islands ($\alpha < \alpha_m$ and $\alpha > \alpha_m$). We also observed the increase in anisotropy on increasing α and discussed the interesting behaviour shown by the ratio $\gamma = L_x/L_y$ in the $\alpha < \alpha_m$ region. We then obtained the stability regions for specific cases of Chromium, Erbium and Dysprosium atoms.

In the future, we would like to study interactions between the solitons, investigating soliton-soliton scattering in the 2D plane. Different outcomes are expected depending on the angle between the direction of collision and the direction of polarization of the soliton.

Bibliography

[1] F. Abdullaev and J. Garnier, *Emergent nonlinear phenomena in bose-einstein condensates*, vol. 45, 2008, pp. 25–43.

[2] K. Aikawa, A. Frisch, M. Mark, S. Baier, A. Rietzler, R. Grimm, and F. Ferlaino, *Bose-einstein condensation of erbium*, Physical Review letters, 108 (2012), p. 210401.

[3] U. Al Khawaja, H. Stoof, R. Hulet, K. Strecker, and G. Partridge, *Bright soliton trains of trapped bose-einstein condensates*, Physical Review letters, 89 (2002), p. 200404.

[4] A. Alberucci, C. P. Jisha, N. F. Smyth, and G. Assanto, *Spatial optical solitons in highly nonlocal media*, Physical Review A, 91 (2015), p. 013841.

[5] M. H. Anderson, J. R. Ensher, M. R. Matthews, C. E. Wieman, and E. A. Cornell, *Observation of bose-einstein condensation in a dilute atomic vapor*, Science, 269 (1995), pp. 198–201.

[6] O. Bang, W. Krolikowski, J. Wyller, and J. J. Rasmussen, *Collapse arrest and soliton stabilization in nonlocal nonlinear media*, Physical Review E, 66 (2002), p. 046619.

[7] S. Bose, *Planck's law and the light quantum hypothesis*, Z. Phys, 26 (1924).

[8] C. C. Bradley, C. Sackett, J. Tollett, and R. Hulet, *Evidence of bose-einstein condensation in an atomic gas with attractive interactions*, Physical Review Letters, 75 (1995), p. 1687.

[9] A. Butsch, C. Conti, F. Biancalana, and P. S. J. Russell, *Optomechanical self-channeling of light in a suspended planar dual-nanoweb waveguide*, Physical Review letters, 108 (2012), p. 093903.

[10] C. Chin, R. Grimm, P. Julienne, and E. Tiesinga, *Feshbach resonances in ultracold gases*, Reviews of Modern Physics, 82 (2010), p. 1225.

[11] C. Conti, M. Peccianti, and G. Assanto, *Route to nonlocality and observation of accessible solitons*, Physical Review letters, 91 (2003), p. 073901.

[12] C. Conti, M. Peccianti, and G. Assanto, *Observation of optical spatial solitons in a highly nonlocal medium*, Physical Review Letters, 92 (2004), p. 113902.

[13] F. Dalfovo, S. Giorgini, L. P. Pitaevskii, and S. Stringari, *Theory of bose-einstein condensation in trapped gases*, Reviews of Modern Physics, 71 (1999), p. 463.

[14] K. B. Davis, M.-O. Mewes, M. R. Andrews, N. Van Druten, D. Durfee, D. Kurn, and W. Ketterle, *Bose-einstein condensation in a gas of sodium atoms*, Physical Review Letters, 75 (1995), p. 3969.

[15] F. P. Dos Santos, J. Léonard, J. Wang, C. Barrelet, F. Perales, E. Rasel, C. Unnikrishnan, M. Leduc, and C. Cohen-Tannoudji, *Bose-einstein condensation of metastable helium*, Physical Review Letters, 86 (2001), p. 3459.

[16] R. Eichler, D. Zajec, P. Köberle, J. Main, and G. Wunner, *Collisions of anisotropic two-dimensional bright solitons in dipolar bose-einstein condensates*, Physical Review A, 86 (2012), p. 053611.

[17] A. Einstein, *Quantentheorie des einatomigen idealen gases*.

[18] S. Giovanazzi, A. Görlitz, and T. Pfau, *Tuning the dipolar interaction in quantum gases*, Physical Review Letters, 89 (2002), p. 130401.

[19] A. Griesmaier, J. Werner, S. Hensler, J. Stuhler, and T. Pfau, *Bose-einstein condensation of chromium*, Physical Review Letters, 94 (2005), p. 160401.

[20] K. Huang, *Statistical Mechanics*, 1987.

[21] L. Khaykovich, F. Schreck, G. Ferrari, T. Bourdel, J. Cubizolles, L. D. Carr, Y. Castin, and C. Salomon, *Formation of a matter-wave bright soliton*, Science, 296 (2002), pp. 1290–1293.

[22] W. Królikowski, M. Saffman, B. Luther-Davies, and C. Denz, *Anomalous interaction of spatial solitons in photorefractive media*, Physical Review letters, 80 (1998), p. 3240.

[23] K. Łakomy, R. Nath, and L. Santos, *Spontaneous crystallization and filamentation of solitons in dipolar condensates*, Physical Review A, 85 (2012), p. 033618.

[24] Y. Lamhot, A. Barak, O. Peleg, and M. Segev, *Self-trapping of optical beams through thermophoresis*, Physical Review letters, 105 (2010), p. 163906.

[25] M. Lu, N. Q. Burdick, S. H. Youn, and B. L. Lev, *Strongly dipolar bose-einstein condensate of dysprosium*, Physical Review letters, 107 (2011), p. 190401.

[26] M. Ma and Z. Huang, *Bright soliton solution of a gross–pitaevskii equation*, Applied Mathematics Letters, 26 (2013), pp. 718–724.

[27] W. Man, S. Fardad, Z. Zhang, J. Prakash, M. Lau, P. Zhang, M. Heinrich, D. N. Christodoulides, and Z. Chen, *Optical nonlinearities and enhanced light transmission in soft-matter systems with tunable polarizabilities*, Physical Review letters, 111 (2013), p. 218302.

[28] F. Maucher, N. Henkel, M. Saffman, W. Królikowski, S. Skupin, and T. Pohl, *Rydberg-induced solitons: three-dimensional self-trapping of matter waves*, Physical Review letters, 106 (2011), p. 170401.

[29] S. Minardi, F. Eilenberger, Y. Kartashov, A. Szameit, U. Röpke, J. Kobelke, K. Schuster, H. Bartelt, S. Nolte, L. Torner, et al., *Three-dimensional light bullets in arrays of waveguides*, Physical Review letters, 105 (2010), p. 263901.

[30] G. Modugno, G. Ferrari, G. Roati, R. Brecha, A. Simoni, and M. Inguscio, *Bose-einstein condensation of potassium atoms by sympathetic cooling*, Science, 294 (2001), pp. 1320–1322.

[31] R. Nath, P. Pedri, and L. Santos, *Soliton-soliton scattering in dipolar bose-einstein condensates*, Physical Review A, 76 (2007), p. 013606.

[32] A. C. Newell, *Solitons in mathematics and physics*, SIAM, 1985.

[33] M. Peccianti and G. Assanto, *Nematicons*, Physics Reports, 516 (2012), pp. 147–208.

[34] M. Peccianti, K. A. Brzdkiewicz, and G. Assanto, *Nonlocal spatial soliton interactions in nematic liquid crystals*, Optics letters, 27 (2002), pp. 1460–1462.

[35] P. Pedri and L. Santos, *Two-dimensional bright solitons in dipolar bose-einstein condensates*, Physical Review Letters, 95 (2005), p. 200404.

[36] O. Penrose and L. Onsager, *Bose-einstein condensation and liquid helium*, Physical Review, 104 (1956), p. 576.

[37] L. Pitaevskii and S. Stringari, *Bose-einstein condensation*, 2003.

[38] P. P. R. Nath and L. Santos, *Phonon instability with respect to soliton formation in two-dimensional dipolar bose-einstein condensates*, Physical Review Letters, 102 (2009), p. 050401.

[39] L. Santos, G. Shlyapnikov, and M. Lewenstein, *Roton-maxon spectrum and stability of trapped dipolar bose-einstein condensates*, Physical Review letters, 90 (2003), p. 250403.

[40] M.-f. Shih, M. Segev, and G. Salamo, *Three-dimensional spiraling of interacting spatial solitons*, Physical Review letters, 78 (1997), p. 2551.

[41] S. Skupin, M. Saffman, and W. Krolikowski, *Nonlocal stabilization of nonlinear beams in a self-focusing atomic vapor*, Physical Review letters, 98 (2007), p. 263902.

[42] A. W. Snyder and D. J. Mitchell, *Accessible solitons*, Science, 276 (1997), pp. 1538–1541.

[43] K. E. Strecker, G. B. Partridge, A. G. Truscott, and R. G. Hulet, *Formation and propagation of matter-wave soliton trains*, Nature, 417 (2002), pp. 150–153.

[44] I. Tikhonenkov, B. Malomed, and A. Vardi, *Anisotropic solitons in dipolar bose-einstein condensates*, Physical Review Letters, 100 (2008), p. 090406.

[45] S. Yi and L. You, *Trapped condensates of atoms with dipole interactions*, Physical Review A, 63 (2001), p. 053607.

Appendix A

List of useful Integrals

$$\int_{-\infty}^{\infty} dx e^{-ax^2} = \sqrt{\frac{\pi}{a}} \tag{A.1}$$

$$\int_{-\infty}^{\infty} dx x^{2n} e^{-ax^2} = \frac{(2n-1)!!}{(2\pi)^n}\sqrt{\frac{\pi}{a}} \tag{A.2}$$

$$\int_{0}^{\infty} dx x^{(2n+1)} e^{-ax^2} = \frac{n!}{2a^{n+1}} \tag{A.3}$$

$$\int_{-\infty}^{\infty} dx x^{(2n+1)} e^{-ax^2} = 0 \tag{A.4}$$

$$\int_{-\infty}^{\infty} dx \frac{1}{x^2+b^2} e^{-ax^2} = \frac{\pi}{b} e^{ab^2} erfc(\sqrt{a}b) \tag{A.5}$$

$$\int_{0}^{\infty} dx x^2 e^{-ax^2} erfc(bx) = \frac{-\sqrt{a}b + (a+b^2)\cot^{-1}\left(\frac{b}{\sqrt{a}}\right)}{2\sqrt{\pi}a^{3/2}(a+b^2)} \tag{A.6}$$

Appendix B

Long Calculations

B.1 Calculation of DDI term in the Energy

Eq. 3.14:

$$
\begin{aligned}
E &= \int d\mathbf{r}\left[\frac{\hbar^2}{2m}|\nabla\Psi(\mathbf{r})|^2 + V_{ext}(\mathbf{r})|\Psi(\mathbf{r})|^2 + \frac{g}{2}|\Psi(\mathbf{r})|^4\right] \\
&\quad + \frac{1}{2}\int d^3\mathbf{r}'\, V_d(\mathbf{r}-\mathbf{r}')\,|\Psi(\mathbf{r})|^2\,|\Psi(\mathbf{r}')|^2 \qquad \text{(B.1)} \\
E_{g_d} &= \frac{1}{2}\int d^3\mathbf{r}'\, V_d(\mathbf{r}-\mathbf{r}')\,|\Psi(\mathbf{r})|^2\,|\Psi(\mathbf{r}')|^2 \qquad \text{(B.2)} \\
&= \frac{1}{2}\int d^3r\; n(r)\frac{1}{(2\pi)^3}\int d^3k\;\tilde{n}(k)\tilde{V}_d(k)e^{i\bar{k}\cdot\bar{r}} \\
&= \frac{1}{2}\int \frac{d^3k}{(2\pi)^3}\tilde{n}^2(k)\tilde{V}_d(k) \\
&= \frac{1}{2}\frac{1}{(2\pi)^3}\int d^3k e^{-\frac{k_\rho^2\cos^2\theta l_z^2L_x^2}{2}-\frac{k_\rho^2\sin^2\theta l_z^2L_y^2}{2}-\frac{k_z^2l_z^2L_z^2}{2}}\frac{4\pi}{3}g_d \\
&\qquad \times\left[\frac{3(k_\rho^2\cos^2\theta\sin^2\alpha + k_\rho k_z\cos\theta\sin 2\alpha + k_z^2\cos^2\alpha)}{k_\rho^2+k_z^2}-1\right] \\
&= \frac{1}{2}\frac{g_d}{6\pi^2}\int dk_\rho k_\rho e^{-\frac{k_\rho^2\cos^2\theta l_z^2L_x^2}{2}-\frac{k_\rho^2\sin^2\theta l_z^2L_y^2}{2}}d\theta dk_z e^{-\frac{k_z^2l_z^2L_z^2}{2}} \\
&\qquad \times\left[\frac{3(k_\rho^2\cos^2\theta\sin^2\alpha + k_\rho k_z\cos\theta\sin 2\alpha + k_z^2\cos^2\alpha)}{k_\rho^2+k_z^2}-1\right]
\end{aligned}
$$

Doing the dk_z integral first,

$$
\begin{aligned}
&= \int_{-\infty}^{\infty} dk_z e^{-\frac{k_z^2 l_z^2 L_z^2}{2}} \left[\frac{3(k_\rho^2 \cos^2\theta \sin^2\alpha + k_\rho k_z \cos\theta \sin 2\alpha + k_z^2 \cos^2\alpha)}{k_\rho^2 + k_z^2} - 1 \right] \\
&= 3k_\rho^2(\cos^2\theta \sin^2\alpha - \cos^2\alpha) \int_{-\infty}^{\infty} dk_z \frac{1}{k_\rho^2 + k_z^2} e^{-\frac{k_z^2 l_z^2 L_z^2}{2}} \\
&\quad +3k_\rho \cos\theta \sin 2\alpha \int_{-\infty}^{\infty} dk_z \frac{k_z}{k_\rho^2 + k_z^2} e^{-\frac{k_z^2 l_z^2 L_z^2}{2}} + (3\cos^2\alpha - 1) \int_{-\infty}^{\infty} dk_z e^{-\frac{k_z^2 l_z^2 L_z^2}{2}} \\
&= 3k_\rho^2(\cos^2\theta \sin^2\alpha - \cos^2\alpha) \frac{\pi}{k_\rho} e^{\frac{k_\rho^2 l_z^2 L_z^2}{2}} \mathrm{Erfc}\left(\frac{k_\rho l_z L_z}{\sqrt{2}} \right) + (3\cos^2\alpha - 1) \frac{\sqrt{2\pi}}{l_z L_z}
\end{aligned}
$$

Therefore,

$$
\begin{aligned}
2E_{g_d} &= \frac{g_d}{2\pi} \int_0^{\infty} dk_\rho k_\rho^2 d\theta e^{-\frac{k_\rho^2 \cos^2\theta l_z^2 L_x^2}{2} - \frac{k_\rho^2 \sin^2\theta l_z^2 L_y^2}{2}} (\cos^2\theta \sin^2\alpha - \cos^2\alpha) \\
&\qquad \times e^{\frac{k_\rho^2 l_z^2}{2}} \mathrm{Erfc}\left(\frac{k_\rho l_z L_z}{\sqrt{2}} \right) \\
&\quad +(3\cos^2\alpha - 1) \frac{\sqrt{2\pi}}{l_z L_z} \frac{g_d}{6\pi^2} \int_0^{\infty} dk_\rho k_\rho d\theta e^{-\frac{k_\rho^2 \cos^2\theta l_z^2 L_x^2}{2} - \frac{k_\rho^2 \sin^2\theta l_z^2 L_y^2}{2}} \\
&= I_1 + I_2 \\
I_2 &= (3\cos^2\alpha - 1) \frac{\sqrt{2\pi}}{l_z L_z} \frac{g_d}{6\pi^2} \int_{-\infty}^{\infty} dk_x e^{-\frac{k_x^2 l_z^2 L_x^2}{2}} \int_{-\infty}^{\infty} dk_y e^{-\frac{k_y^2 l_z^2 L_y^2}{2}} \\
&= \frac{g_d}{6\pi^2} (3\cos^2\alpha - 1) \frac{\sqrt{2\pi}}{l_z L_z} \frac{\sqrt{2\pi}}{l_z L_x} \frac{\sqrt{2\pi}}{l_z L_y} \\
&= \sqrt{\frac{2}{\pi}} \frac{g_d}{3} \frac{(3\cos^2\alpha - 1)}{l_z^3 L_x L_y L_z} \\
I_1 &= \frac{g_d}{2\pi} \int_0^{\infty} dk_\rho k_\rho^2 d\theta e^{-\frac{k_\rho^2 \cos^2\theta l_z^2 L_x^2}{2} - \frac{k_\rho^2 \sin^2\theta l_z^2 L_y^2}{2}} (\cos^2\theta \sin^2\alpha - \cos^2\alpha) \\
&\qquad \times e^{\frac{k_\rho^2 l_z^2}{2}} \mathrm{Erfc}\left(\frac{k_\rho l_z L_z}{\sqrt{2}} \right) \\
&= \frac{g_d}{2\pi} \int_0^{2\pi} d\theta (\cos^2\theta \sin^2\alpha - \cos^2\alpha) \int_{-\infty}^{\infty} dk_\rho k_\rho^2 e^{-\frac{k_\rho^2 l_z^2}{2}(\cos^2\theta L_x^2 + \sin^2\theta L_y^2 - L_z^2)} \\
&\qquad \times \mathrm{Erfc}\left(\frac{k_\rho l_z L_z}{\sqrt{2}} \right) \\
&= \frac{g_d}{2\pi} \sqrt{\frac{2}{\pi}} \frac{1}{l_z^3} \int_0^{2\pi} d\theta (\cos^2\theta \sin^2\alpha - \cos^2\alpha) \cdot A
\end{aligned}
$$

$$
\begin{aligned}
A &= \frac{1}{(\cos^2\theta L_x^2+\sin^2\theta L_y^2-L_z^2)}\Bigg[\frac{-L_z}{(\cos^2\theta L_x^2+\sin^2\theta L_y^2)} \\
&\quad +\frac{1}{\sqrt{\cos^2\theta L_x^2+\sin^2\theta L_y^2-L_z^2}}tan^{-1}\left(\frac{\sqrt{\cos^2\theta L_x^2+\sin^2\theta L_y^2-L_z^2}}{L_z}\right)\Bigg] \\
I_{1a} &= -\frac{g_d}{2\pi}\sqrt{\frac{2}{\pi}}\frac{1}{l_z^3}L_z\int_0^{2\pi}d\theta\frac{(\cos^2\theta\sin^2\alpha-\cos^2\alpha)}{(\cos^2\theta L_x^2+\sin^2\theta L_y^2-L_z^2)}\frac{1}{(\cos^2\theta L_x^2+\sin^2\theta L_y^2)} \\
&= -\frac{g_d}{2\pi}\sqrt{\frac{2}{\pi}}\frac{1}{l_z^3}L_z\frac{2\pi}{L_z^2}\Bigg[\cos^2\alpha\left(\frac{1}{L_xL_y}-\frac{1}{\sqrt{(L_x^2-L_z^2)(L_y^2-L_z^2)}}\right) \\
&\quad +\frac{\sin^2\alpha}{L_x^2-L_y^2}\left(\frac{L_y}{L_x}-\sqrt{\frac{L_y^2-L_z^2}{L_x^2-L_z^2}}\right)\Bigg] \\
&= -\frac{g_d}{l_z^3}\sqrt{\frac{2}{\pi}}\frac{1}{L_z}\Bigg[\cos^2\alpha\left(\frac{1}{L_xL_y}-\frac{1}{\sqrt{(L_x^2-L_z^2)(L_y^2-L_z^2)}}\right) \\
&\quad +\frac{\sin^2\alpha}{L_x^2-L_y^2}\left(\frac{L_y}{L_x}-\sqrt{\frac{L_y^2-L_z^2}{L_x^2-L_z^2}}\right)\Bigg] \\
I_{1b} &= \frac{g_d}{2\pi}\sqrt{\frac{2}{\pi}}\frac{1}{l_z^3}\int_0^{2\pi}d\theta\frac{(\cos^2\theta\sin^2\alpha-\cos^2\alpha)}{(\cos^2\theta L_x^2+\sin^2\theta L_y^2-L_z^2)^{3/2}} \\
&\qquad \times tan^{-1}\left(\frac{\sqrt{\cos^2\theta L_x^2+\sin^2\theta L_y^2-L_z^2}}{L_z}\right)
\end{aligned}
$$

Scaling g and g_d we get,

$$
\begin{aligned}
\frac{E_{g_d}}{\hbar\omega_z} &= \frac{\tilde{g}_d}{3L_z}\left[\frac{3\cos^2\alpha}{\sqrt{(L_x^2-L_z^2)(L_y^2-L_z^2)}}-\frac{3\sin^2\alpha}{L_x^2-L_y^2}\left(\frac{L_y}{L_x}-\sqrt{\frac{L_y^2-L_z^2}{L_x^2-L_z^2}}\right)-\frac{1}{L_xL_y}\right] \\
&\quad +\frac{\tilde{g}_d}{2\pi}\int_0^{2\pi}d\theta\frac{(\cos^2\theta\sin^2\alpha-\cos^2\alpha)}{(\cos^2\theta L_x^2+\sin^2\theta L_y^2-L_z^2)^{3/2}} \\
&\qquad \times tan^{-1}\left(\frac{\sqrt{\cos^2\theta L_x^2+\sin^2\theta L_y^2-L_z^2}}{L_z}\right) \qquad \text{(B.3)}
\end{aligned}
$$

B.2 Calculation of DDI term in Lagrangian 3.18

$$
\begin{aligned}
L_{g_d} &= \frac{1}{2}|\psi|^2 \int dr' V_d(r-r')|\psi(r')|^2 \qquad \text{(B.4)}\\
&= \frac{A^4}{2}\int dr \int dr' V_d(r-r') \prod_{\eta,\eta'} e^{-\frac{(\eta-\eta_0(t))^2}{w_\eta^2(t)}} e^{-\frac{(\eta'-\eta_0(t))^2}{w_\eta^2(t)}}\\
&= \frac{A^4}{2}\int dr \int dr' V_d(r-r') \prod_{x,y,z} e^{-\frac{\eta^2+\eta'^2-2\eta_0(\eta+\eta')+2\eta_0^2}{w_\eta^2}}\\
&= \frac{A^4}{2}\int dr_c \prod_{x,y,z} e^{-\frac{2\eta_c^2}{w_\eta^2}} \int dr_r V_d(r_r) \prod_{x,y,z} e^{-\frac{(\eta_r-2\eta_0)^2}{2w_\eta^2}}\\
&= \frac{1}{2(2\pi)^{3/2}w_x w_y w_z}\int dr_r V_d(r_r) \prod_{x,y,z} e^{-\frac{\eta_r^2}{2w_\eta^2}}\\
&= \frac{g_d}{2}\frac{4\pi}{3}\frac{1}{(2\pi)^3}\int dk(3\cos^2\theta_{k.d}-1) \prod_{\eta=x,y,z} e^{-\frac{k_\eta^2 w_{\eta 2}}{2}} \qquad \text{(B.5)}
\end{aligned}
$$

B.3 Calculation of DDI term in μ 3.4

$$
\begin{aligned}
\mu_{DDI} &= \int dz|\phi(z)|^2 \int d^3r' V_d^{3D}(\bar{r}-\bar{r'})|\psi(\bar{r'})|^2 \qquad \text{(B.6)}\\
&= \int dz|\phi(z)|^2 \int \frac{d^3k}{(2\pi)^3}\tilde{V}_d(k)\tilde{n}(k)e^{ik\cdot r}\\
&= \int dz|\phi(z)|^2 \int \frac{d^3k}{(2\pi)^3}\tilde{V}_d(k)n_0(2\pi\delta(k_x))(2\pi\delta(k_y))e^{-\frac{k_z^2 l_z^2}{4}}e^{ik\cdot r}\\
&= \frac{n_0}{2\pi}\int dz|\phi(z)|^2 \int dk_x dk_y dk_z \delta(k_x)\delta(k_y)e^{-\frac{k_z^2 l_z^2}{4}}e^{ik\cdot r}\frac{4\pi}{3}g_d\\
&\qquad \times\left[\frac{3(k_x^2\sin^2\alpha + k_z k_x \sin 2\alpha + k_z^2\cos^2\alpha)}{k_x^2+k_y^2+k_z^2}-1\right]\\
&= \frac{n_0}{2\pi}\frac{4\pi}{3}g_d\int dz|\phi(z)|^2\int dk_z e^{-\frac{k_z^2 l_z^2}{4}}e^{ik_z z}\left[\frac{3(k_z^2\cos^2\alpha)}{k_z^2}-1\right]\\
&= \frac{2n_0}{3}\frac{(3\cos^2\alpha-1)}{\sqrt{\pi}l_z}g_d\int dz e^{-\frac{z^2}{l_z^2}}\int_{-\infty}^{\infty}dk_z e^{-\frac{z^2}{l_z}}e^{-\frac{l_z^2}{4}\left(k_z-\frac{2iz}{l_z^2}\right)^2}\\
&= \frac{2n_0}{3}\frac{(3\cos^2\alpha-1)}{\sqrt{\pi}l_z}g_d\frac{2\sqrt{\pi}}{l_z}l_z\sqrt{\frac{\pi}{2}}\\
&= \frac{2}{3}\sqrt{2\pi}\frac{g_d}{l_z}n_0(3\cos^2\alpha-1) \qquad \text{(B.7)}
\end{aligned}
$$